

Review

Materials and chemistry design for low-temperature all-solid-state batteries

Pushun Lu,^{1,2} Zhimin Zhou,^{1,3} Zuxiang Xiao,⁴ Jiaze Lu,⁵ Jiaxu Zhang,^{1,2} Guantai Hu,^{1,2} Wenlin Yan,⁵ Shengjie Xia,^{1,3} Shutao Zhang,¹ Ziqing Wang,¹ Hong Li,⁵ Changhong Wang,^{1,*} Fan Wu,^{5,*} and Xueliang Sun^{1,*}

SUMMARY

All-solid-state batteries (ASSBs) have garnered significant interest due to their exceptional safety features and high theoretical energy density. Despite extensive research demonstrating the impressive electrochemical performance of ASSBs at moderate and high temperatures, their electrochemical performance significantly degrades in a cold environment, with the underlying mechanism yet to be disclosed. In this review, we examine the ion transport kinetics of ASSBs and emphasize the challenges they face at low temperatures. By examining microscopic kinetic processes, including Li-ion migration within solid electrolytes (SEs), interfacial charge transfer, and bulk electrode diffusion, we outline the critical challenges and specific requirements on SEs, interfaces, and electrodes for low-temperature ASSBs. Based on these insights, a range of materials and chemistry design strategies for high-performance ASSBs at low temperatures are reviewed. Finally, future research directions for improving low-temperature ASSB performance are proposed. This study aims to offer a thorough understanding and crucial insights to improve the low-temperature performance of ASSBs.

INTRODUCTION

The impending requirement for clean and sustainable energy, along with the flourishing advancement of electric vehicles and energy storage stations, resulted in the widespread application of energy storage devices, specifically lithium-ion batteries (LIBs).^{1,2} However, the limited energy density and disconcerting safety issues significantly impede the development and application of LIBs.³ In contrast to commercialized LIBs with organic liquid electrolytes (OLEs), all-solid-state batteries (ASSBs) employing solid electrolytes (SEs) possess superior energy density⁴ and improved safety,^{5–7} thus being regarded as the next-generation energy storage technology and garnering significant attention from academia and industry.⁸

Over the past years, substantial efforts have been devoted to developing SEs, designing SE/electrode interfaces, and engineering all-solid-state pouch cells. Nowadays, the room-temperature ionic conductivity of SE is over 10 mS cm⁻¹, such as Li₁₀GeP₂S₁₂ (LGPS, 12 mS cm⁻¹),⁹ Li_{9.54}Si_{1.74}P_{1.44}S_{11.7}Cl_{0.3} (25 mS cm⁻¹),¹⁰ Li_{9.54}[Si_{0.6}Ge_{0.4}]_{1.74}P_{1.44}S_{11.1}Br_{0.3}O_{0.6} (LSiGePSBrO) (32 mS cm⁻¹),¹¹ LiTaOCl₄ (12.4 mS cm⁻¹),¹² and LiNbOCl₄ (10.4 mS cm⁻¹).¹² Various interface design strategies^{13–15} have been demonstrated to effectively suppress solid-solid interfacial resistance. With remarkable advancements in SEs and solid-solid interfaces, ASSBs have now shown exceptional electrochemical performance within moderate

CONTEXT & SCALE

All-solid-state batteries have been recognized as a promising technology to address the energy density limits and safety issues of conventional Li-ion batteries that employ organic liquid electrolytes. Over the past years, remarkable progress has been achieved at moderate and high temperatures, while the low-temperature operation of all-solid-state batteries emerges as a critical challenge that restricts their wide temperature application. In this context, we discuss the microscopic kinetic processes, outline the challenges and requirements for low-temperature operation, highlight the materials and chemistry design strategies, and propose the future directions to enhance the performance at cold environments, especially from the perspective of solid electrolytes, interface, and electrodes. This review aims to provide valuable insights to advance the low-temperature application of all-solid-state batteries.



(20°C–30°C)^{10,16–18} and elevated (40°C–70°C)^{10,19,20} temperature ranges, such as fast charging and discharging, high areal capacity, long-term cycling stability, and high power density. However, when exposed to low-temperature environments, such as the deep ocean, outer space, and the high latitudes of the northern and southern hemispheres, ASSBs suffer from significant degradation in electrochemical performance, thus restricting their practical application in cold conditions. Besides, the underlying mechanism of inferior performance of low-temperature ASSBs remains unclear.

In this comprehensive review, we first delve into the ion transport kinetic process of ASSBs and emphasize the challenges encountered at low temperatures, including sluggish Li⁺ migration in SE, retarded charge transfer at SE/electrode interface, and Li⁺ solid-state diffusion in electrode. Besides, we outline specific requirements for SEs, interfaces, and electrodes. Based on these insightful understandings, effective materials and chemistry design strategies are systematically reviewed. Last but not least, current challenges as well as future directions aimed at advancing low-temperature performance of ASSBs are proposed. This comprehensive review aims to offer valuable insights for improving the low-temperature performance of ASSBs.

GLOBAL SURFACE TEMPERATURE DISTRIBUTION IN WINTER

According to the global climate data (Figure 1A), a general trend of increasing latitude correlating with decreasing temperature is observed.²¹ In particular, areas with average winter minimum temperatures below 0°C constitute 47.95% of the total land area (Figure 1B). The area percentage for various temperature ranges of –20°C to 0°C, –40°C to –20°C, –60°C to –40°C, –80°C to –60°C, and below –80°C account for 17.97%, 20.29%, 7.37%, 2.13%, and 0.18%, respectively. This temperature gradient distribution leads to diverse temperature requirements in various application scenarios (Figure 1C), including deep-sea operations (0°C), civil applications (–30°C), military applications (–50°C), polar expeditions (–80°C), and space missions (–100°C).^{22–24} Besides terrestrial environments, the deep ocean and outer space can experience even more extreme cold temperatures. Hence, developing ASSBs with outstanding low-temperature performance is essential for their widespread application.

KINETIC PROCESSES AND CHALLENGES OF LOW-TEMPERATURE ASSBs

Kinetic processes

At low temperatures, the critical factor that limits the electrochemical performances of batteries has been considered to be the sluggish kinetics of Li⁺.^{23,25,26} Consequently, before seeking effective strategies to improve the low-temperature performances, it is necessary to understand the kinetic processes in ASSBs. For the simplest situation, these kinetic processes can be classified into three main steps (Figure 2): (1) Li⁺ migration in SE, (2) interfacial charge transfer at electrode/SE interface, and (3) Li⁺ diffusion in the bulk electrode. Given the complexity of actual ASSBs configurations, it is necessary to discuss these microscopic kinetic processes in detail.

Li⁺ is the unique carrier of inorganic SEs (e.g., oxide, sulfide, halide) with immobile sublattice, resulting in a transference number close to unity.²⁷ In terms of the polycrystalline inorganic SEs (e.g., LGPS), Li⁺ migration consists of the transport in grain/bulk and grain boundary (top of Figure 2). From the macroscopic level, the ionic conductivity of crystalline inorganic SEs abides by the Arrhenius equation:

¹Eastern Institute for Advanced Study, Eastern Institute of Technology, Ningbo 315200, China

²University of Science and Technology of China, Hefei 230026, China

³Shanghai Jiao Tong University, Shanghai 200240, China

⁴Shenzhen Data Management Center of Planning and Natural Resource, Shenzhen 518034, China

⁵Institute of Physics, Chinese Academy of Sciences, Beijing 100190, China

*Correspondence: cwang@eitech.edu.cn (C.W.), fwu@iphy.ac.cn (F.W.), xsun@eitech.edu.cn (X.S.)

<https://doi.org/10.1016/j.joule.2024.01.027>

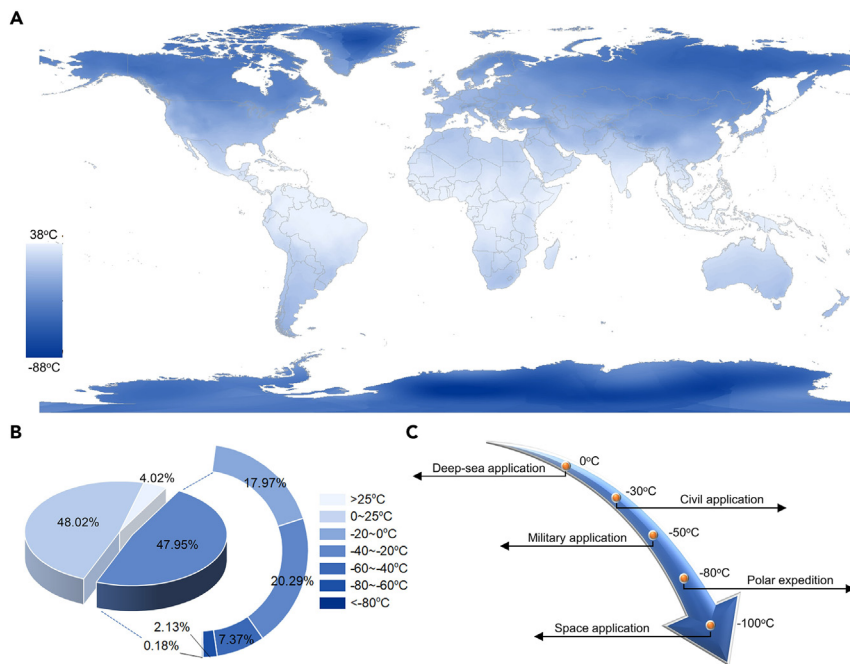


Figure 1. Global average winter minimum temperature

(A) Global distribution of average winter minimum temperature (2020–2022). The original data come from the National Center for Environmental Information (NCEI) of the National Oceanic and Atmospheric Administration (NOAA) (<https://www.ncdc.noaa.gov/global-summary-of-the-day/archive/>).

(B) Area percentage for various temperature ranges of >25°C, 0°C–25°C, -20°C to 0°C, -40°C to -20°C, -60°C to -40°C, -80°C to -60°C, and <-80°C.

(C) Temperature limit requirements under various application scenarios.

$$\sigma = \frac{\sigma_0}{T} e^{-\frac{E_a}{k_B T}} \quad (\text{Equation 1})$$

Where σ , σ_0 , T , k_B , and E_a are the ionic conductivity, pre-exponential factor, absolute temperature, Boltzmann constant, and activation energy, respectively. The activation energy E_a determines the sensitivity of ionic conductivity to the temperature variation. Drawing on the present insights, E_a is influenced by multi-scale factors,^{28,29} such as interactions of charges, lattice defects and migration modes at the atomic scale, lattice volume and bottlenecks, structural frustration and disorder and lattice dynamics at the crystal structure scale, and grain boundary effect at the microstructure scale. Currently, the strategies to reduce the activation energy may only hold for specific scale or certain materials. For instance, the rotational dynamics of polyhedra that can promote the ion hopping has merely been observed in specific polyanions.³⁰ Consequently, it is more advisable to determine the optimal approaches for lowering the activation energy based on the critical features of the crystalline inorganic SEs.

As for amorphous inorganic SEs (e.g., Li₂S-P₂S₅ glass), Li⁺ migration only involves the transport in bulk. The ionic conductivity of amorphous inorganic SE follows the Vogel-Tamman-Fulcher (VTF) equation:

$$\sigma = A T^{-\frac{1}{2}} e^{-\frac{E_a}{T-T_0}} \quad (\text{Equation 2})$$

Where A is the pre-exponential factor, and T_0 is the equilibrium glass transition temperature that is close to the glass transition temperature. However, within the

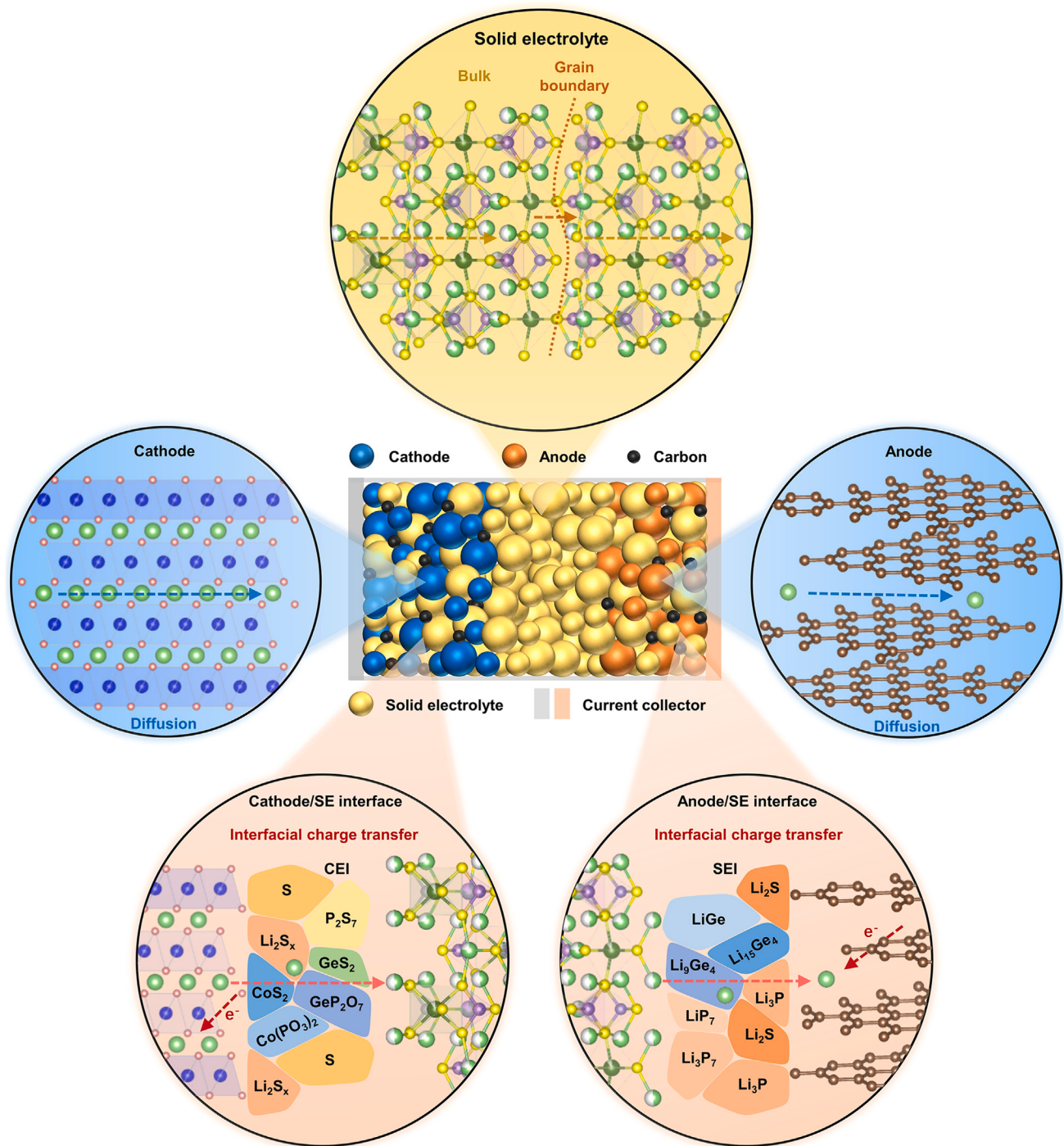


Figure 2. Kinetic processes in ASSBs

Top: Li^+ migration in polycrystalline inorganic SEs involving the transport in grain/bulk and grain boundary.

Center left: Li^+ diffusion in bulk cathode.

Center: schematic of ASSBs using inorganic SEs.

Center right: Li^+ diffusion in bulk anode.

Bottom left: interfacial charge transfer process at cathode/SE interface.

Bottom right: interfacial charge transfer process at anode/SE interface.

practical test temperature region that is much lower than the glass transition temperature (e.g., >200°C) of amorphous inorganic SEs, the temperature-dependent relationship can be approximated to the Arrhenius relationship.³¹ According to the Anderson-Stuart (A-S) model,³² the activation energy E_a is contributed by the binding energy E_b and the electrostatic strain energy E_s , as described by [Equation 3](#).

$$E_a = E_b + E_s \quad (\text{Equation 3})$$

Where E_b denotes the energy for separating the Li⁺ from the network, and E_s represents the energy for opening up the bottleneck/doorway in the structure for the ions to pass through. For instance, through the introduction of bridging oxygen rather than bridging sulfur into the oxysulfide glass,³³ the Li⁺ conduction path can be expanded, thus decreasing the activation energy.

Notably, Li⁺ of polymer SEs (e.g., polyethylene oxide [PEO]-based SEs) may partially exist in the form of weak solvation apart from the interaction with polar groups of the chain segments, and its transference number is relatively lower since the motion of anions dissociated from lithium salts is inevitable.³⁴ If the polymer SE can be regarded as a homogeneous and isotropic material, Li⁺ motion can also be simplified into the transport in bulk. Since pure polymer SEs with relatively low glass transition temperatures belong to the amorphous system, their ionic conductivity also conforms to the VTF equation. Based on the current understandings, diminishing the polymer interchain interaction, as well as weakening the interactions involving the polymer's polar group-Li⁺ and anion-Li⁺ are the directions to reduce the activation energy.³⁵ As for the composite SEs, such as the combination of polymer SE and inorganic filler, the migration of Li⁺ will become more complicated, involving the transport in bulk polymer SE or inorganic filler (if it is ion conductive) and their interfaces.^{36,37}

The interfacial kinetic process (bottom of [Figure 2](#)) in ASSBs comprises multiple steps, including (1) Li⁺ transport across SE/interphase interface after extrication from the sublattice or coordination environment of SE, (2) Li⁺ diffusion through interphase, and (3) charge transfer at electrode surface, which are collectively referred to as interfacial charge transfer process.³⁸ As the solvation structure of Li⁺ is absent in inorganic SEs, the energy-consuming desolvation process of Li⁺ existing at the OLE/interphase interface should not appear in ASSBs using inorganic SEs. However, since the understanding of the SE/interphase interface is vacant, it is uncertain whether a similar but undetected process exists at the SE/interphase interface and whether Li⁺ transport across this interface needs to overcome the analogous energy barrier. Moreover, the physicochemical properties of the interphase consisting of all-inorganic components should be distinct from the mosaic-type solid electrolyte interphase (SEI) with inorganic and organic hybrid components in LIBs. Consequently, how all-inorganic interphase impacts the Li⁺ transport and follow-up charge transfer is indeterminate.

In recent years, many electrode materials investigated in LIBs have been applied to ASSBs configurations. Take the intercalation-type cathode as an instance, the diffusion process (left and right middle of [Figure 2](#)) and kinetics in this kind of cathode should be unchanged. Nevertheless, it is still crucial to reveal underlying mechanisms that are decisive to low-temperature performances under ASSB configurations. For instance, the lithium storage mechanisms and kinetics of different electrodes (e.g., intercalation-type, conversion-type, and pseudocapacitive electrodes) at low temperatures should be systematically investigated in the future.

Therefore, more efforts are required to deepen the understanding of microscopic kinetic processes in ASSBs, based on which the improvement in low-temperature or other (e.g., fast charge and discharge) performances will be more efficient.

Low-temperature challenges and fundamental requirements

With decreasing temperature, almost all temperature-dependent kinetic processes become sluggish. Therefore, the low-temperature performance improvement is a systematic project associated with all kinetic processes in batteries. However, among all kinetic processes, the rate-limiting process with the slowest kinetics determines the low-temperature performances of ASSBs to a great extent. In light of this, regulating the kinetics of the rate-limiting process can achieve the most significant improvement.^{25,39} Considering the distinct kinetic processes of ASSBs with solidified SE separator and electrode/SE interface, it is necessary to perform special identification on the rate-limiting step. Recently, based on the semi-quantitative analysis from distribution of relaxation times (DRT),⁴⁰ Lu et al.⁴¹ thought that Li⁺ conduction among SE (Li₆PS₅Cl [LPSC]) particles is the rate-limiting process at extremely low temperatures (e.g., from -60°C to -40°C), while the solid-state diffusion in bulk electrode and charge transfer process at electrode/SE interface play a dominant role at relatively high temperature (e.g., -20°C to 30°C) under the configuration of Swagelok model cells. Unfortunately, it has not reached a consensus on the rate-limiting process in ASSBs nowadays. In addition, the challenges or limitations suffered by ASSBs have not been comprehensively recognized.

Therefore, based on currently limited understandings, the challenges of low-temperature ASSBs are summarized here. (1) The drop of ionic conductivity with decreasing temperature is still serious, although the freezing issue can be prevented by replacing OLEs with SEs. (2) Besides, large interfacial resistance originated from unstable interface or unfavorable interphases may substantially limit the low-temperature performances improvement. (3) More importantly, since the interfacial contact (i.e., "solid-solid" contact) issue has not been well addressed at mild temperature and even under large stacking pressure, it may further aggravate the degradation of electrochemical performances at low temperature. (4) The poor electronic conductivity of cathode surface compromises the charge transfer kinetics to some extent, as the employment of carbon additive that may accelerate the decomposition of SEs and deteriorate the interface stability is advisable to be avoided. (5) Moreover, the inherited active materials from LIBs are required to be further designed to realize high diffusion coefficient in solid-state electrode.

To realize high electrochemical performances of ASSB operating at low temperatures, fundamental requirements for the design on battery materials and chemistry are proposed accordingly: (1) maintaining high ionic conductivity of SE at extremely low temperature, so that fast ion transport in SE layer can be held, (2) maintaining low interphase resistance, (3) maintaining good interfacial contact, (4) maintaining high electronic conductivity of the electrode surface without compromising interface stability, and (5) maintaining high ionic diffusivity of electrode. In the following sections, materials and chemistry design strategies that attempt to satisfy aforementioned requirements for low-temperature ASSBs are reviewed in detail in the order of SE, interface, and electrode.

LOW-TEMPERATURE SE DESIGN

The prerequisite to support low-temperature operation of batteries is maintaining high ionic conductivity. In contrast to the freezing of OLEs at subzero temperatures,

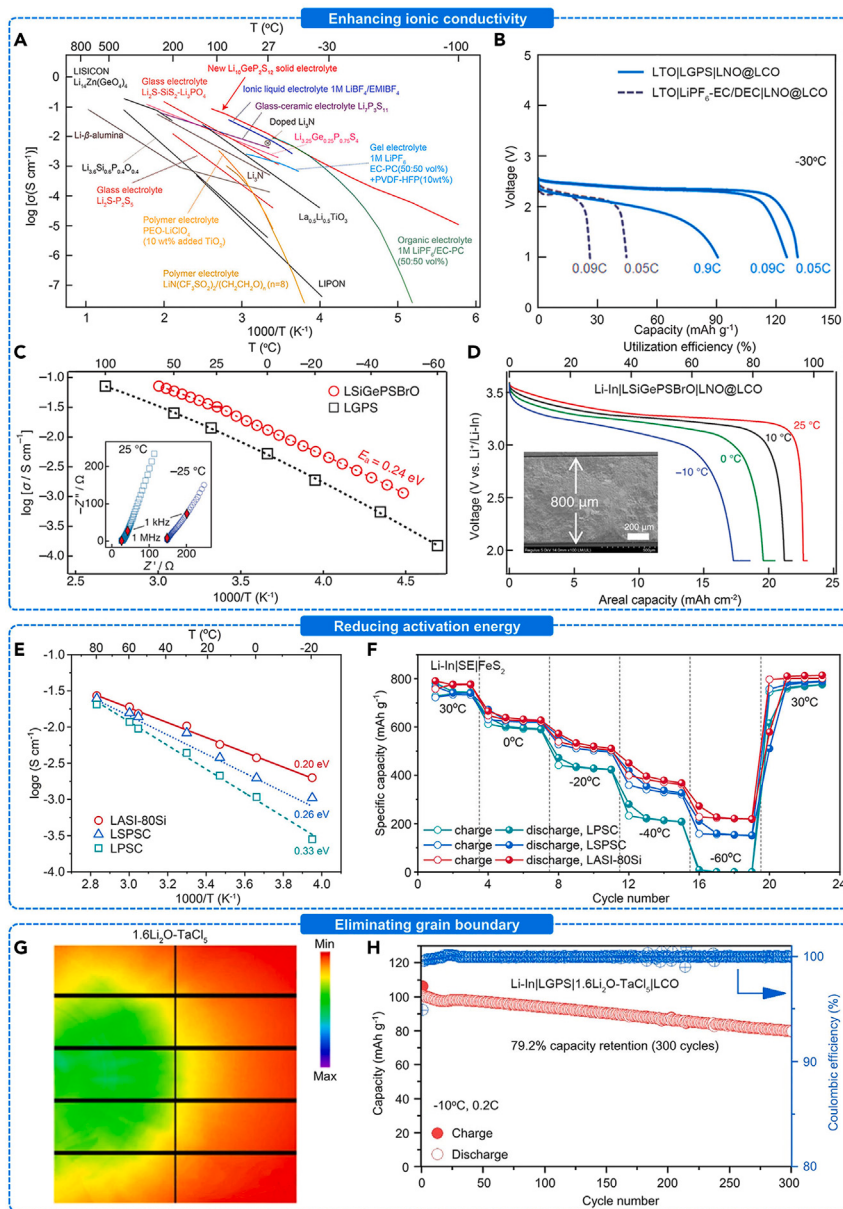


Figure 3. Low-temperature inorganic solid electrolytes design

(A) Arrhenius plots for the ionic conductivities of various representative electrolytes (adapted from Kamaya et al.⁹ with permission. Copyright 2011, Springer Nature).

(B) Discharge curves of Li₄Ti₅O₁₂|LGPS|LiCoO₂ ASSB and Li₄Ti₅O₁₂|LiPF₆-EC(ethylene carbonate)/DEC(diethyl carbonate)|LiCoO₂ LIB at -30°C and different current rates of 0.05C, 0.09C, and 0.9C (adapted from Kato et al.¹⁰ with permission. Copyright 2016, Springer Nature).

(C) Arrhenius plots for the bulk conductivities of Li_{9.54}[Si_{0.6}Ge_{0.4}]_{1.74}P_{1.44}S_{11.1}Br_{0.3}O_{0.6} and LGPS. Inset: typical impedance plots measured at -25°C (right) and 25°C (left) (adapted from Li et al.¹¹ with permission. Copyright 2023, The Authors).

(D) Discharge curves for the thick electrode presented herein (~800 μm) under 0.587 mA cm⁻² (0.025C) at different temperatures ranging from 25°C to -10°C. Inset: cross-sectional scanning electron microscopy image of the cathode composite pellet with a capacity loading of 23.5 mAh cm⁻² (adapted from Li et al.¹¹ with permission. Copyright 2023, The Authors).

(E) Arrhenius plots for the ionic conductivities of Li_{6.8}Si_{0.8}As_{0.2}S₅ (LASI-80Si), Li_{9.54}Si_{1.74}P_{1.44}S_{11.1}Cl_{0.3} (LSPSC) and Li₆PS₅Cl (LPSC) SEs (adapted from Lu et al.¹² with permission. Copyright 2022, John Wiley and Sons).

Figure 3. Continued

(F) Charge-discharge curves for Li-In|SE|FeS₂ ASSBs at various temperatures from -60°C to 30°C (adapted from Lu et al.⁴¹ with permission. Copyright 2022, John Wiley and Sons).

(G) Synchrotron-based 2D diffraction images of 1.6Li₂O-TaCl₅ amorphous halide SE (adapted from Zhang et al.⁴² with permission. Copyright 2023, The Authors).

(H) Cycle performance of Li-In|1.6Li₂O-TaCl₅|LiCoO₂ ASSB at -10°C (adapted from Zhang et al.⁴² with permission. Copyright 2023, The Authors).

SEs preserve solid state over a wide temperature range without the complete loss of ion-conducting function, which ought to be one of potential advantages. However, in the past decades, strenuous efforts have been made to elevate the ionic conductivity of SEs at mild temperature, while rare attention has been paid to ponder over how to attain satisfactory ionic conductivity at low temperature.

Inorganic SEs

Consistently improving room-temperature ionic conductivity of SEs should be the simple and direct way. In 2011, Kamaya et al.⁹ developed a lithium superionic conductor LGPS with ionic conductivity of 12 mS cm⁻¹, which is comparable to that of commercialized OLEs of LIBs. As shown in Figure 3A, while the ionic conductivity of OLEs undergoes a dramatic drop at -30°C as a result of the increased viscosity, poor wettability and possible freezing issue, LGPS retains a decent ionic conductivity of ~1 mS cm⁻¹. Accordingly, Li₄Ti₅O₁₂ (LTO)||LiCoO₂ (LCO) ASSB with LGPS SE displays superior capacity output to the counterpart using commercialized OLEs (Figure 3B).¹⁰ Lately, based on the LGPS-type crystal structure, Li et al.¹¹ designed a high-entropy composition LSiGePSBrO through both anion and cation substitution, realizing a record-breaking ionic conductivity of 32 mS cm⁻¹. Although LSiGePSBrO has a similar activation energy (0.24 eV) to LGPS, it retains an ionic conductivity of ~1 mS cm⁻¹ even at -50°C (Figure 3C). Consequently, this high-entropy superionic conductor can enable a millimeter-thick electrode to work at -10°C. Impressively, the areal capacity at -10°C reaches ~17 mAh cm⁻², which is still 75% of that at 25°C (Figure 3D). Therefore, improving ionic conductivity is a direct but effective way applicable to not only mild temperature but also low-temperature conditions to promote the electrochemical performances of ASSBs.

Reducing activation energy is another way to diminish the sensitivity of ionic conductivity to temperature variation and preserve high ionic conductivity at subzero temperatures since the ionic conductivity of most superionic conductors conforms to the Arrhenius or VTF relationship. For instance, Lu et al.⁴³ reported that the activation energy of Li_{6.8}Si_{0.8}As_{0.2}S₅I (LASI-80Si) SE could be significantly reduced through Si substitution and resulting concerted migration mechanism. Although LASI-80Si has a similar room-temperature ionic conductivity to LSPSC (cold-pressed pellet, 10.2 mS cm⁻¹), its lower activation energy (0.20 eV) results in a delayed decline of ionic conductivity at sub-zero temperatures⁴¹ (Figure 3E). As a result, FeS₂ ASSB with LASI-80Si can operate at extremely low temperature of -60°C and exhibit superior capacity than that of LSPSC (Figure 3F). In stark contrast, the substantially decreased ionic conductivity of LSPSC SE originated from large activation energy (0.33 eV) interrupts the capacity output at -60°C. Following closely behind, Yu et al.⁴⁴ employed Li₇P₃S₁₁ glass-ceramic with inferior room-temperature ionic conductivity of 1.27 mS cm⁻¹ as the SE to assemble Li-In|Li₇P₃S₁₁|FeS₂ ASSB, resulting in a reduced specific capacity at 0°C.

Eliminating or alleviating the effect of huge grain boundary resistance especially for oxide SEs can promote the migration of Li⁺ inside SE. Owing to the good deformability and absent grain boundary,⁴⁵ amorphous SEs have been considered as promising materials to achieve compact separators. Recently, Zhang et al.⁴² reported that

1.6Li₂O-TaCl₅ oxychloride amorphous SE with vague-halo diffraction patterns (Figure 3G) exhibits an impressive ionic conductivity of 6.6 mS cm⁻¹ at 25°C, which is comparable to that of crystalline SEs.¹² Accordingly, Li-In|LGPS|1.6Li₂O-TaCl₅|LCO ASSB with this amorphous SE demonstrates a long cycle life (300 cycles) at -10°C (Figure 3H).

Polymer SEs

Due to the distinct chemical components and resulting physicochemical properties from inorganic counterparts, polymer SEs have distinctive design strategies. PEO and its derivatives as representative polymer SEs show excellent mechanical flexibility, low cost, and facile processability.⁴⁶ However, the high crystallinity of the PEO matrix and resulting inadequate ionic conductivities (10⁻⁸ to 10⁻⁶ S cm⁻¹) at room temperature impel the operation temperature to be ≥60°C, which substantially blocks the way to subzero temperatures to some extent.

Consequently, reducing the crystallinity of PEO-based SEs turns into the major direction to achieve sufficient ionic conductivity at lower working temperature. While Li_{6.4}La₃Zr_{1.4}Ta_{0.6}O₁₂ (LLZTO) fillers can reduce the crystallinity of PEO matrix from 37.2% to 31.4%, the incorporation of succinonitrile (SN) plasticizer (Figure 4A) can achieve a minimum of 8.4%.⁴⁷ In addition, compared with the limited effect of LLZTO filler on the room-temperature ionic conductivity, the addition of SN plasticizer can further boost the ionic conductivity to 7.66 × 10⁻⁴ S cm⁻¹ (Figure 4B, LLZTO-incorporated polymer solid electrolyte with 60 wt% or X wt% of PEO (LCPE-60 or LCPE-X)). Accordingly, Li||LiFePO₄ (LFP) ASSB with LCPE-60 exhibits good cyclic stability at -10°C. However, adding plasticizers often compromises the mechanical strength of PEO-based SEs. In light of this, Lv et al.⁴⁸ considered that cross-linking was an alternative strategy to realize both reduced crystallinity and enhanced mechanical strength. By ultraviolet (UV) polymerizing PEO and methacryloyloxypropyltrimethoxy silane (KH570)-modified SiO₂ (named as KS) (Figure 4C), cross-linking networks can be successfully established, thus contributing to a high ionic conductivity at room (3.37 × 10⁻⁴ S cm⁻¹) and low (1.73 × 10⁻⁴ S cm⁻¹ at 0°C) temperature. Consequently, Li||LFP ASSB with the composite SE (named as KSCE) can steadily cycle for 150 cycles at 0.2C and 0°C (Figure 4D).

In order to obtain a comprehensive understanding, low-temperature performances of other potential polymer SEs apart from PEO-based SEs are necessary to be investigated. Significantly, Lin and Liu⁴⁹ designed a starch-based SE, in which the starch host is constructed by two cross-linking reactions. As the schematic shows in Figure 4E, γ-(2,3-epoxypropoxy)-propyltrimethoxy-silane (KH560) as a larger cross-linker reacts with starch first and BH₃ as a smaller cross-linker continues to cross-link with the residual -OH groups. Based on this design, BstSi SE possesses decent ionic conductivity (Figure 4F) at 25°C (3.10 × 10⁻⁴ S cm⁻¹), 0°C (1.23 × 10⁻⁴ S cm⁻¹) and -20°C (3.10 × 10⁻⁵ S cm⁻¹), thus enabling Li||LFP ASSB operate at 0°C and -20°C (Figure 4G).

Although several strategies have been applied to improve the low-temperature ionic conductivity of SEs in recent years, the universal design principles to realize superionic conductivity and the combined strategies over multiple scales to harvest the minimized activation energy are still required. Learning from the development experience of low-temperature OLEs (e.g., the understanding of solvation structure and desolvation energy), the interaction of Li⁺ carriers with surrounding coordination structure or anion framework, and the effect of grain boundary or other defects on Li⁺ transport should be seriously examined especially under low-temperature conditions.

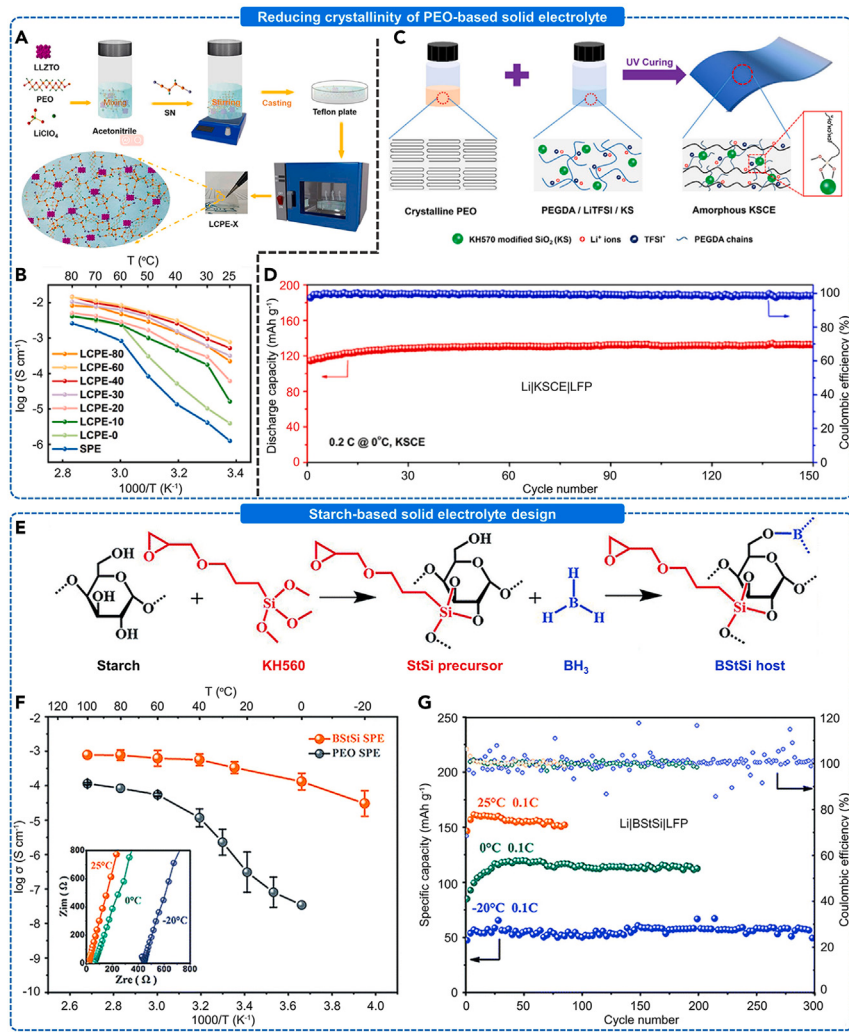


Figure 4. Low-temperature polymer solid electrolytes design

- (A) Preparation procedure of LCPE-X with SN plasticizer (adapted from Zhang et al.⁴⁷ with permission. Copyright 2023, Elsevier).
- (B) Temperature-dependent ionic conductivities of LCPE-X (X = 0, 10, 20, 30, 40, 60, 80) and polymer solid electrolyte (also named as solid polymer electrolyte [SPE] in the legend) (adapted from Zhang et al.⁴⁷ with permission. Copyright 2023, Elsevier).
- (C) Preparation procedure of amorphous KSCE (adapted from Lv et al.⁴⁸ with permission. Copyright 2021, Elsevier).
- (D) Cycle performance of Li|KSCE|LFP at 0.2C and 0°C (adapted from Lv et al.⁴⁸ with permission. Copyright 2021, Elsevier).
- (E) Schematic of the preparation of starch-based polymer SE (SPE) through two-step cross-linking reactions (adapted from Lin and Liu⁴⁹ with permission. Copyright 2019, Royal Society of Chemistry).
- (F) Temperature-dependent ionic conductivities of BStSi polymer SE (SPE) and PEO polymer SE (SPE) (adapted from Lin and Liu⁴⁹ with permission. Copyright 2019, Royal Society of Chemistry).
- (G) Cycle performances of Li|BStSi|LFP at 0.1C and different working temperatures of 25°C, 0°C, -20°C (adapted from Lin and Liu⁴⁹ with permission. Copyright 2019, Royal Society of Chemistry).

LOW-TEMPERATURE INTERFACE DESIGN

The interface of ASSBs is very complicated, arising from a combination of factors, such as the interaction of multiple interphases, intricate structures and electrochemical/chemical reactions at the microscopic scale, and the influence of experimental conditions (e.g., current density) and external environments (e.g., temperature,

pressure). A thorough understanding of these complexities is crucial for achieving high-performance ASSBs. Although the Li^+ transport from the electrolyte to the electrode surface is generally defined as an interfacial charge transfer process, the actual kinetic process occurring at the SE/electrode interface is multiple. Learning from the understanding on the interface of LIBs, the interfacial kinetic processes in ASSBs should consist of the transport of Li^+ across SE/interphase interface, the diffusion of Li^+ across interphase, the charge transfer at interphase/electrode interface (or electrode surface). In light of this, the low-temperature interface design strategies can be classified into three kinds, i.e., SE/interphase interface modulation, interphase modification and charge transfer kinetics regulation. Indeed, the latter two strategies have been implemented to improve the low-temperature performances of ASSBs. But unfortunately, as the understanding on SE/interphase interface is vacant, the corresponding strategy is lacking. Since the solvation structure of Li^+ is absent in SE, the energy-consuming desolvation process of Li^+ existing at OLEs/interphase interface should not appear in ASSBs. However, it is uncertain whether a similar but undetected process exists at SE/interphase interface and Li^+ transport across this interface needs to overcome analogous energy barrier. More importantly, the interfacial contact (i.e., solid-solid contact) issue especially for ASSBs using inorganic SEs may aggravate the deterioration of electrochemical performances at low temperature, given that it has not been well resolved at mild temperature and even large stacking pressure. Therefore, based on recent progress achieved, the low-temperature interface design will be discussed from three aspects, i.e., interphase modification, electronic conductivity tuning, and interfacial contact enhancement.

Interphase modification

An ideal interphase should be electrochemically/chemically stable, ion conductive, electron insulative, flexible, and intimate with electrode. Unfortunately, most of interphases *in situ* formed at SE/electrode interface are generally undesired. For this reason, designing an artificial interphase is a common strategy. For instance, a coating layer (e.g., LiNbO_3) is usually constructed at the surface of high-voltage oxide cathode to suppress side reactions between cathode and sulfide SEs. Morino⁵⁰ investigated the impact of LiNbO_3 coating layer on the low-temperature performance of $\text{LiNi}_{0.5}\text{Co}_{0.2}\text{Mn}_{0.3}\text{O}_2$ (NCM523) ASSB. As shown in Figure 5A, LiNbO_3 -coated NCM523 cathode presents superior discharge capacity to the uncoated one at each subzero temperature. After equivalent-circuit fitting (Figure 5B), resistances from SE separator (R_1), interphase component (R_2), charge transfer at cathode surface layer (R_3) can be identified (Figure 5C). As expected, the resistance R_1 and its activation energy is exactly the same for both uncoated and coated samples, according to the Arrhenius plots shown in Figure 5D. The resistance R_3 and associated activation energy of LiNbO_3 -coated NCM523 sample are substantially reduced compared with those of the uncoated sample. Due to the suppression of side reactions, it is reasonable to conclude that the charge transfer process at cathode surface can be facilitated. Interestingly, the resistance R_2 of the coated sample becomes larger, while its activation energy is decreased. It is speculated that the low value of R_2 for the uncoated sample may be induced by the surface residual lithium compounds, such as LiOH and Li_2CO_3 . Peng et al.⁵⁴ also demonstrated that LiNbO_3 coating layer could stabilize $\text{LiNi}_{0.7}\text{Co}_{0.1}\text{Mn}_{0.2}\text{O}_2$ (NCM712) cathode/sulfide SE interface and suppress some resistances (i.e., resistances from cathode/SE and anode/SE) increase at subzero temperatures, compared with that of the uncoated sample. However, it is inconceivable that the resistance from anode/SE interface can be influenced by the cathode coating layer. Notably, the thickness⁵⁵ and components⁵⁶ of coating layer also have influences on the kinetics of Li^+ passing through

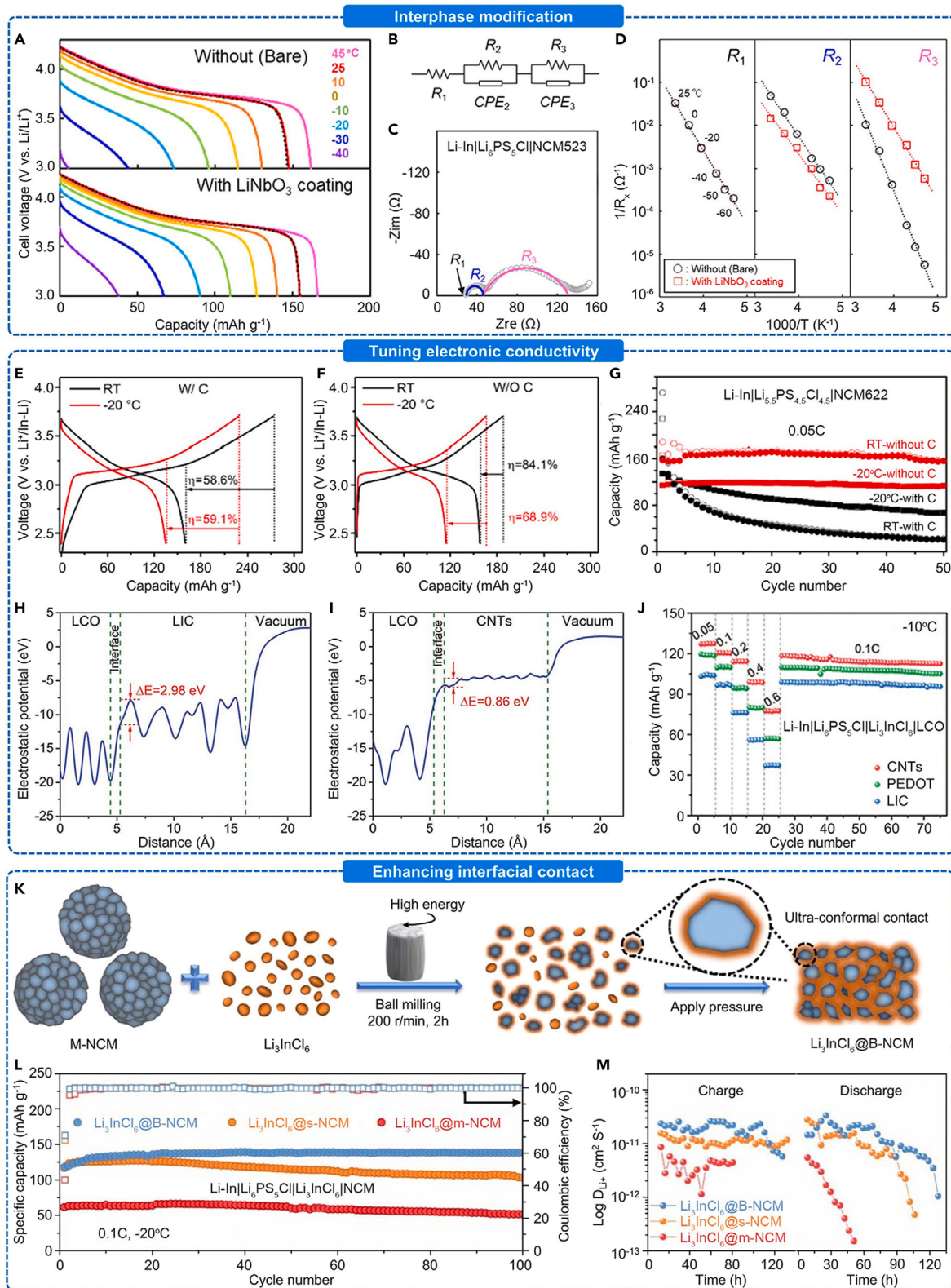


Figure 5. Low-temperature interface design

- (A) Discharge curves of Li-In/Li₆PS₅Cl/NCM523 ASSBs with bare and LiNbO₃-coated NCM523 cathode at various temperatures from 45°C to -40°C (adapted from Morino⁵⁰ with permission. Copyright 2022, The Authors).
- (B) The equivalent circuit model used for fitting (adapted from Morino⁵⁰ with permission. Copyright 2022, The Authors).
- (C) The Nyquist plot of Li-In/Li₆PS₅Cl/NCM523 ASSB after equivalent circuit fitting (adapted from Morino⁵⁰ with permission. Copyright 2022, The Authors).
- (D) The resistance-temperature relationships of resistance R₁, R₂, and R₃ (adapted from Morino⁵⁰ with permission. Copyright 2022, The Authors).
- (E) Charge-discharge curves of Li-In|Li_{5.5}PS_{4.5}Cl_{1.5}|NCM622 ASSB without the addition of carbon additive in composite NCM622 cathode at room temperature and -20°C (adapted from Peng et al.⁵¹ with permission. Copyright 2022, Elsevier).
- (F) Charge-discharge curves of Li-In|Li_{5.5}PS_{4.5}Cl_{1.5}|NCM622 ASSB with the addition of carbon additive in composite NCM622 cathode at room temperature and -20°C (adapted from Peng et al.⁵¹ with permission. Copyright 2022, Elsevier).
- (G) Cycle performances of Li-In|Li_{5.5}PS_{4.5}Cl_{1.5}|NCM622 ASSBs with/without the addition of carbon additive in composite NCM622 cathode at 0.05C and room temperature or -20°C (adapted from Peng et al.⁵¹ with permission. Copyright 2022, Elsevier).
- (H) The electrostatic potential profiles for LCO/LIC interface (adapted from Deng et al.⁵² with permission. Copyright 2022, John Wiley and Sons).
- (I) The electrostatic potential profiles for LCO/CNTs interface (adapted from Deng et al.⁵² with permission. Copyright 2022, John Wiley and Sons).
- (J) The rate capability performances of Li-In|Li₆PS₅Cl|Li₃InCl₆|LCO ASSBs with/without the utilization of CNTs or PEDOT in composite LCO cathode at various current rates from 0.05 to 0.6C and -10°C (adapted from Deng et al.⁵² with permission. Copyright 2022, John Wiley and Sons).
- (K) Schematic of the preparation procedure of Li₃InCl₆@B-NCM (adapted from Zhang et al.⁵³ with permission. Copyright 2023, Royal Society of Chemistry).
- (L) Cycle performances of Li-In|Li₆PS₅Cl|Li₃InCl₆|NCM ASSBs using Li₃InCl₆@B-NCM, Li₃InCl₆@s-NCM, and Li₃InCl₆@m-NCM cathodes, respectively, at 0.1C and -20°C (adapted from Zhang et al. with permission⁵³. Copyright 2023, Royal Society of Chemistry).
- (M) Diffusion coefficient (D_{Li+}) of different cathodes at -20°C (adapted from Zhang et al.⁵³ with permission. Copyright 2023, Royal Society of Chemistry).

interphase, which remain to be further investigated under low-temperature condition. In terms of the anode side, Li et al.⁵⁷ delicately designed a dual-layered SEI that consists of amorphous Li_xBO_yF_z outer layer and LiF-rich inner layer on the Li metal electrode, along with small amount of organic species, Li₂CO₃ and Li₂O. Benefiting from the low energy barrier for Li⁺ diffusion, the Li⁺ transfer across this SEI is enhanced and the Li deposition becomes more uniform even at low temperatures. Consequently, the Li||NCM811 coin cell delivers high capacity (92 mAh g⁻¹) at -30°C and the lowest operation temperature of the polymer-based Li||NCM811 pouch cell reaches -48.2°C. Therefore, it is crucial to elucidate the correlation between the components and the kinetics of interphases at low temperature, aiming to develop effective interphase modification strategies.

Apart from the electrode/SE interface, the interface of current collector with cathode or SE is also important, which is rarely noticed. Notably, due to the existence of halogen,⁵⁸ the reaction of halide SE with Al foil current collector is serious, which leads to the corrosion of Al foil and decomposition of halide SE.⁵⁹ Accordingly, Deng et al.⁵⁹ performed a modification on the Al foil through graphene-like carbon coating to separate LIC SE and Al foil current collector, thus suppressing the side reactions. Besides, this modification also enhances the charge transfer kinetics at the interface of current collector, thus enabling Li-In/Li₆PS₅Cl/Li₃InCl₆/LCO ASSB with high discharge capacity and stable cycle at 0.05C and -10°C.

Therefore, the interphase modification is crucial for the interfacial stability, as well as the low-temperature electrochemical performances of ASSBs. Nevertheless, the influences of physicochemical properties (e.g., ionic and electronic conductivity, chemical components, thickness, and deformability) of interphase layer on the low-temperature performances of ASSBs remain to be further investigated.

Electronic conductivity tuning

Apart from the ionic conductivity, the electronic conductivity at cathode surface also has significant impact on the charge transfer kinetics. However, previous reports^{60,61} have disclosed that increased electronic conductivity of electrode through adding conductive carbon additive may accelerate the decomposition of SEs, thus jeopardizing the interfacial stability. Specifically, Peng et al.⁵¹ discovered that

$\text{LiNi}_{0.6}\text{Co}_{0.2}\text{Mn}_{0.2}\text{O}_2$ (NCM622) composite cathode with carbon additive displayed lower initial Coulombic efficiency (Figure 5E) than that without carbon additive (Figure 5F), regardless of the temperature (either room temperature or -20°C). Besides, the addition of carbon additive also deteriorates the cyclic stability (Figure 5G) of sulfide-based ASSBs due to the enhanced degradation reactions occurring at the NCM/SE and carbon/SE interfaces.^{62,63} To overcome the detrimental effect of conventional carbon additives, Deng et al.⁶⁴ designed a poly(3,4-ethylenedioxythiophene) (PEDOT) coated carbon nanotubes (CNTs) as the semiconductive additive applied in the cathode composites with sulfide SE. It reveals that the PEDOT modification not only substantially mitigates the side reactions but also attains effective electron transfer at the cathode/SE/carbon three-phase interface. In stark contrast to the sulfide SE in composite cathode, Deng et al.⁵² found that the decomposition of halide SE could be significantly suppressed at -10°C even with the utilization of CNTs. As the electrochemical oxidation stability of halide SEs far exceed sulfide SEs, the moderate electronic conductivity at low temperature is insufficient to catalyze halide SE decomposition. Based on the calculated electrostatic potentials, the charge transfer kinetics of LCO composite cathode with CNTs (Figure 5I) is superior to that without CNTs (Figure 5H), thus resulting in a substantially improved rate capability at -10°C (Figure 5J).

Therefore, when tuning the electronic conductivity of composite electrode to elevate low-temperature performances of ASSBs, both interfacial stability and charge transfer kinetics should be taken into account.

Interfacial contact improvement

The interfacial contact issue remains a great challenge especially for ASSBs with inorganic SEs. On one hand, pores preexist inside the polycrystalline cathodes, since SEs have no fluidity and wettability like OLEs to fill these voids. On the other hand, the insufficient flexibility of SEs may lead to abundant pores and physical contact loss inside the solid composite electrode during assembly and cycle. At cold environments, the drop of ionic conductivity and the possible variation of Young's modulus⁶⁵ may further magnify the adverse impact of limited interfacial contact on electrochemical performances.

Peng et al.⁶⁶ found that reducing the particle size of sulfide SE ($\text{Li}_{5.5}\text{PS}_{4.5}\text{Cl}_{1.5}$) in the composite cathode could improve the solid/solid contact area between active materials (NCM712) and sulfide SE, thus enhancing the lithium-ion transport. Interestingly, the configuration (S/L) coupling small-size (S) SE in composite cathode and large-size (L) SE in the electrolyte layer shows superior electrochemical performance at room temperature and -20°C to those of other configurations (S/S, L/L, and L/S). Subsequently, under the $\text{Li}-\text{In}|\text{Li}_2\text{P}_2\text{S}_{8|0.5}\text{Cl}_{0.5}|3\text{Li}_2\text{S}-\text{LiI}$ ASSB configuration with conversion-type cathode, Wu et al.⁶⁷ discovered that the physical contact is more intimate at 0°C than that at room temperature and 60°C , with respect to both cathode/SE interface and interface between composite cathode layer and SE separator layer. Due to the limited depth of charge and discharge at low temperature, $3\text{Li}_2\text{S}-\text{LiI}$ cathode suffers from smaller volume change, preventing the formation of considerable cracks. Lately, Zhang et al.⁵³ designed an ultra-conformal interface between polycrystalline Ni-rich NCM cathode and halide SE (Li_3InCl_6) through high-energy mechanical ball milling (Figure 5K). Thanks to the sufficient physical contact without noticeable voids and cracks, lithium ions transport more quickly (Figure 5M) in the composite cathode ($\text{Li}_3\text{InCl}_6@\text{B-NCM}$) with ultra-conformal interface at -20°C . In addition to superior specific capacity, ASSB with ultra-conformal cathode interface also displays outstanding stability with a capacity retention of 99.6% after cycling

at 0.1C and -20°C for 100 cycles (Figure 5L). In contrast, due to the poor physical contacts, composite cathode ($\text{Li}_3\text{InCl}_6@\text{m-NCM}$) prepared by hand grinding micro-meter-sized NCM cathode and Li_3InCl_6 SE delivers inferior specific capacity and cyclic stability. Notably, Lee et al.¹⁹ reported that the warm isostatic press (WIP) technology can enhance the mechanical strength of SE film owing to the increased density. Subsequently, they further applied WIP after pouch cell assembly and stacking to improve the solid-solid interfacial contacts, thereby resulting in a lower stacking pressure of 2 MPa during operation without sacrificing electrochemical performances. Compared with sulfide and halide SEs, oxide SEs (e.g., LLZTO) possess extremely high Young's modules and resulting poor physical contacts with oxide cathodes. Even after special interfacial treatment (e.g., quick liquid phase sintering⁶⁸), the discharge capacity of $\text{Li}||\text{LCO}$ ASSB at 0.05C and 10°C merely reaches $\sim 12 \text{ mAh g}^{-1}$.

Despite the good mechanical flexibility, the *ex situ* synthesized polymer SEs still encounter a high interface resistance as a result of the poor contacts with other cell components. In light of this, Zhao et al.⁶⁹ designed a conformal interfacial contact through the *in situ* polymerization of 1,3-dioxolane (DOL) initiated by cationic aluminum species. Benefiting from the wettability of the liquid precursors, a good interfacial contact with electrode can be created, and then preserved after the polymerization. Lately, Li et al.⁵⁷ demonstrated that the *in-situ*-polymerized SEs using 1,3,5-trioxane-based precursor contributes to fast interfacial charge transfer kinetics and high-capacity retention (>75%) at -20°C . Nevertheless, considering the incomplete polymerization and the residual unpolymerized monomers, it is more advisable to define the configurations based on *in situ* polymerization as the quasi-solid-state batteries. Notably, the mechanical property change of Li metal with decreased temperature⁷⁰ inevitably influences the interfacial contact with SE. Interestingly, Spencer Jolly et al.⁷¹ found that the deformability of Li metal decreases at -20°C , thus requiring a higher stacking pressure to achieve the same Li/SE interfacial contact at 25°C and decrease the charge transfer resistance. Consequently, the mechanical response of battery materials (e.g., Li metal anode and SEs⁷²) and electrode/SE interface to the dropping temperature may become more pivotal especially under ASSB configuration, which remains to be further investigated.

Therefore, enhancing interfacial contact of solid composite electrode plays a crucial role in improving low-temperature performances of ASSBs, whether using inorganic or polymer SEs. Various interfacial treatment methods or strategies need to be further developed, according to the physicochemical properties (e.g., deformability, particle size, volume change during cycle) of SEs and active materials.

LOW-TEMPERATURE ELECTRODE DESIGN

As the electrode can be regarded as an equipotential body, the transport of Li^+ inside the electrode should be a diffusion process driven by concentration gradient. However, owing to the differences on physicochemical properties (e.g., diffusion pathway, channel size, defect, particle size), the diffusion kinetics of Li^+ in different electrodes may be distinct. For instance, olivine-type LFP with one-dimensional (1D) ion channel along the [010] direction brings about the orderly but sluggishly extraction and insertion of Li^+ , while spinel-type LiMn_2O_4 that has three-dimensional (3D) Li^+ conduction pathway is more favorable for low-temperature Li^+ diffusion.²⁶ Proper cationic doping to enhance the diffusion rate of Li^+ and particle size reducing to short the Li^+ migration path are expected to accelerate the diffusion kinetics.

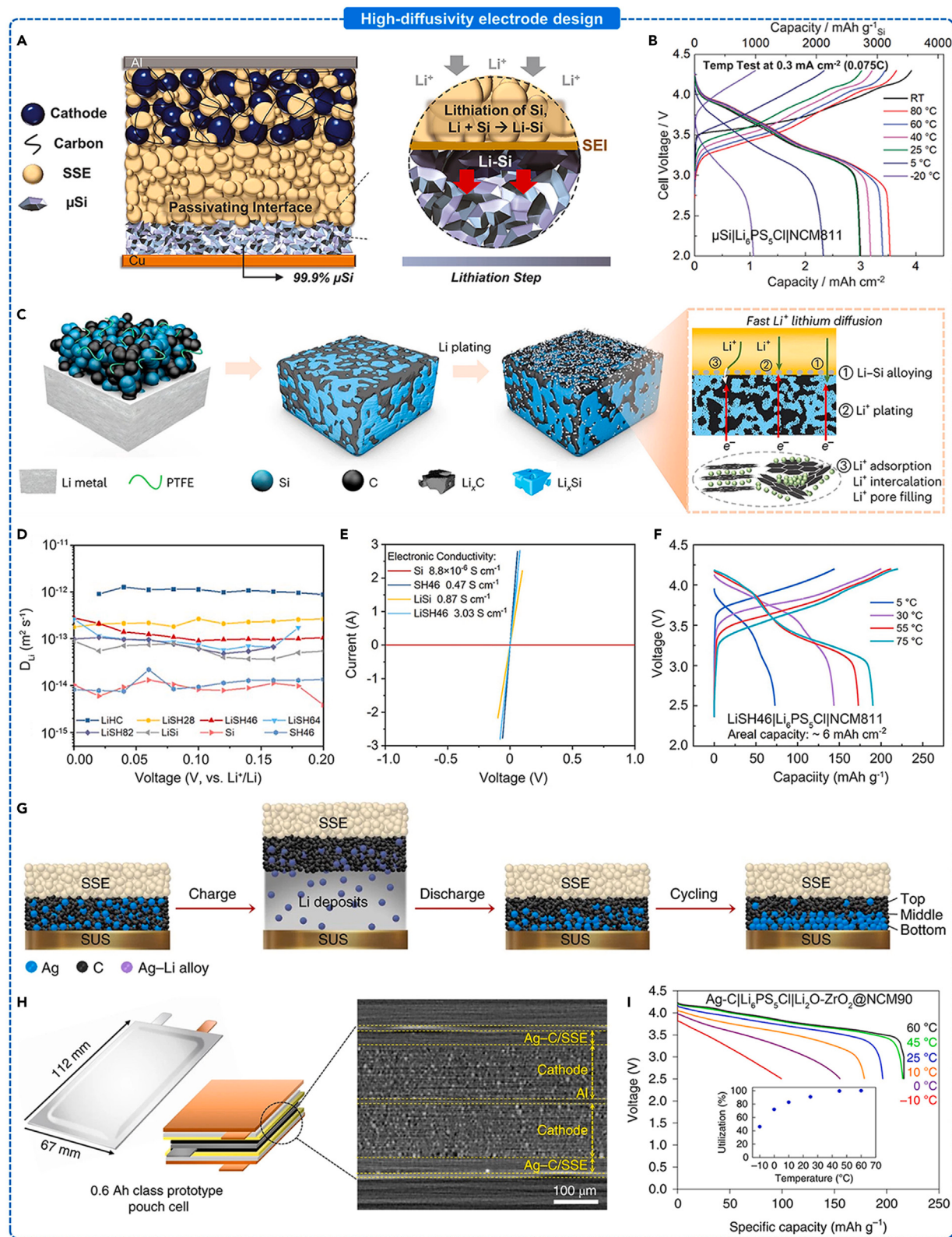


Figure 6. Low-temperature electrode design

- (A) Schematic of $\mu\text{Si}|\text{Li}_6\text{PS}_5\text{Cl}|\text{NCM}811$ ASSB (adapted from Tan et al.⁷⁶ with permission. Copyright 2021, The American Association for the Advancement of Science). During lithiation, a passivating SEI is formed between μSi and $\text{Li}_6\text{PS}_5\text{Cl}$, followed by the lithiation of μSi particles near the interface.
- (B) Wide temperature range (-20°C to 80°C) test of $\mu\text{Si}|\text{Li}_6\text{PS}_5\text{Cl}|\text{NCM}811$ ASSB (adapted from Tan et al.⁷⁶ with permission. Copyright 2021, The American Association for the Advancement of Science).
- (C) Schematic of hard carbon (HC) stabilized LiSi anode (adapted from Yan et al.⁷⁷ with permission. Copyright 2023, Springer Nature). Inset: due to sintering of Si, LiSH46 is a densely continuous anode with fast lithium diffusion. HC provides the graphene layer, pores, and surface to accommodate excessive lithium and suppress lithium dendrite growth. Inside this anode, a 3D Li-rich Li^+/e^- conducting network is constructed to improve the electrode kinetics and mechanical stability.
- (D) Lithium diffusion coefficient calculated from the potentiostatic intermittent titration technique (PITT) for LiHC, LiSH28, LiSH46, LiSH64, LiSH82, and SH46 anode at 55°C (adapted from Yan et al.⁷⁷ with permission. Copyright 2023, Springer Nature).
- (E) Volt-ampere curves of Si, SH46, LiSi, and LiSH46 anode at 55°C , from which the electronic conductivity was calculated (adapted from Yan et al.⁷⁷ with permission. Copyright 2023, Springer Nature).
- (F) Wide temperature range (5°C – 75°C) test of LiSH46| $\text{Li}_6\text{PS}_5\text{Cl}|\text{NCM}811$ ASSB at 0.1C (adapted from Yan et al.⁷⁷ with permission. Copyright 2023, Springer Nature).
- (G) Schematic of Li plating-stripping on the current collector with an Ag-C nanocomposite layer during charging and discharging processes (adapted from Lee et al.¹⁹ with permission. Copyright 2020, Springer Nature).
- (H) Illustration of a 0.6 Ah class prototype pouch cell (right) and X-ray computed tomography (CT) of the bi-cell and symmetric structure (adapted from Lee et al.¹⁹ with permission. Copyright 2020, Springer Nature).
- (I) Discharge capacities of Ag-C| $\text{Li}_6\text{PS}_5\text{Cl}||\text{Li}_2\text{O}\text{-ZrO}_2$ |NCM90 ASSB pouch cell under 0.1C/0.1C charge/discharge conditions with the discharging temperature decreasing from 60°C to -10°C (adapted from Lee et al.¹⁹ with permission. Copyright 2020, Springer Nature). The charging temperature was fixed at 60°C .

However, low-temperature intercalation-type cathodes adopting these strategies remain to be validated under ASSB configuration. Moreover, amorphous electrode materials^{73,74} have been proposed to overcome the confinement of ordered and rigid crystal structures and thus accelerate the solid-state ion diffusion. Recently, Lu et al.⁷⁵ prepared a sulfur-equivalent cathode $\text{Mo}_{0.5}\text{Ti}_{0.5}\text{S}_4$ with an amorphous structure and enriched sulfur anions by high-energy ball milling. Thanks to the enhanced diffusion kinetics and induced anionic redox chemistry, ASSBs with $\text{Mo}_{0.5}\text{Ti}_{0.5}\text{S}_4$ present excellent low-temperature performances, including good cyclability and rate capability at -20°C , and improved capacity retention (50.7 %) at -40°C .

Regarding the low-temperature anodes, significant progress has been made for the past few years. In 2021, Tan et al.⁷⁶ designed a carbon-free pure (99.9%) microsilicon (μSi) anode to eliminate continuous interfacial growth and irreversible lithium losses. As a result of the impermeability of sulfide SE, the interfacial contact area between sulfide SE and pure Si electrode can be reduced into a two-dimensional (2D) plane even during lithiation/delithiation (Figure 6A). Given the decent electronic conductivity ($10^{-5} \text{ S cm}^{-1}$) of Si as a well-known electronic semiconductor, carbon additive can be removed without compromising the charge transfer kinetics and inducing adverse sulfide SE decomposition. Impressively, the average Li^+ diffusivity reaches $\sim 10^{-9} \text{ cm}^2 \text{ s}^{-1}$, merely relying on the contact among Si particles. Consequently, no short circuit emerges for $\mu\text{Si}|\text{Li}_6\text{PS}_5\text{Cl}|\text{NCM}811$ ASSB during charging at -20°C (Figure 6B). Subsequently, Yan et al.⁷⁷ introduced 60 wt % hard carbon (HC) into μSi anode to construct a faster 3D ionic-electronic conductive network (LiSH46: composite of 40 wt% μSi and 60 wt% HC after pre-lithiation) through pre-lithiation and alleviate lithium dendrite growth and huge volume expansion issues (Figure 6C). Compared with the pristine Si and LiSi alloy anodes, LiSH46 anode exhibits superior ionic (Figure 6D) and electronic conductivity (Figure 6E). Accordingly, LiSH46| $\text{Li}_6\text{PS}_5\text{Cl}|\text{NCM}811$ ASSB presents an areal capacity of 2.3 mAh cm^{-2} at 5°C (Figure 6F), corresponding to a capacity retention of 52.3% (relative to that at 30°C). However, as this complicated anode involves multiple lithium storage mechanisms (e.g., alloying, intercalation, plating, absorption, and pore filling, as depicted in Figure 6C), it is difficult to identify or quantify their kinetics differences at low

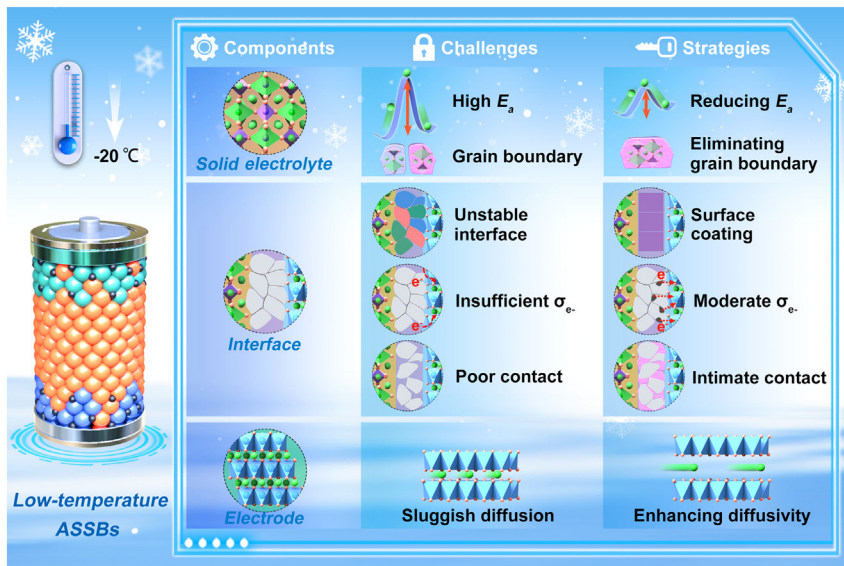


Figure 7. Summary of the critical challenges and effective strategies for low-temperature ASSBs

temperature. In 2020, Lee et al.¹⁹ innovatively designed a lithium-metal-free Ag-C nanocomposite anode to address the undesired lithium dendrite growth and low Coulombic efficiency problems. In addition to provide a highly stable interface by separating lithium with Li₆PS₅Cl (Figure 6G), the amorphous carbon in Ag-C layer also acts as an ionic conductor with high diffusivity of Li⁺. Notably, the Ag-C|Li₆PS₅Cl|Li₂O-ZrO₂@LiNi_{0.90}Co_{0.05}Mn_{0.05} (NCM90) pouch cell (0.6 Ah) with a bi-cell structure (Figure 6H) demonstrates a capacity retention of ~47% at -10°C (Figure 6I). Based on the aforementioned results, it can be concluded that complex structures and diversified components may be the rational design directions to low-temperature anodes with high diffusivity, despite the compromised capacity.

Therefore, numerous factors (e.g., lithium storage mechanisms, diffusion pathway, and particle size of active materials) that influence the electrode performances are required to be investigated in the future, aiming to obtain a comprehensive understanding of low-temperature electrode design.

SUMMARY AND OUTLOOKS

In sum, the research progress in low-temperature ASSBs was systematically reviewed from the aspects of kinetic processes, critical challenges, fundamental requirements, and effective material and chemistry design strategies, as summarized in Figure 7. In terms of kinetic processes, three main steps (Figure 2) have been divided as follows: (1) Li⁺ migration in SE, (2) charge transfer at SE/electrode interface, and (3) Li⁺ diffusion inside the electrode. According to the SE types, Li⁺ migration in SE can be classified into bulk or bulk and grain boundary transport. Owing to the complexity of the SE/electrode interface, the interfacial kinetic process comprises (1) Li⁺ transport across the SE/interphase interface, (2) Li⁺ diffusion through interphase, and (3) charge transfer at the electrode surface. The solid-state Li⁺ diffusion kinetics may be distinct, depending on the properties of the electrodes. Based on the understanding of kinetic processes, the challenges of low-temperature ASSBs can be summarized as the following: (1) the dramatic drop of ionic conductivity of SE with decreasing temperature, (2) large interfacial resistance originating from the unstable interface or unfavorable interphases, (3) limited interfacial contact and

aggravated contact loss issues, (4) insufficient electronic conductivity at electrode surface, and (5) sluggish solid-state Li⁺ diffusion in electrode materials. To overcome these challenges, a series of materials and chemistry design strategies regarding SEs, SE/electrode interfaces and electrodes have been developed. At the level of SEs, reducing activation energy and grain boundary resistance of SE are favorable to maintaining high ionic conductivity at low temperature apart from improving room-temperature ionic conductivity. At the SE/electrode interface, interphase modification, electronic conductivity modulation, and interfacial contact enhancement have been proposed to enhance the interfacial kinetics at low temperature. In terms of solid-state electrodes, high-diffusivity electrodes (e.g., μSi and LiSH46 anode) have been designed even without the assistance of SE. Accordingly, based on these strategies, significant progress has been made in the improvement of low-temperature performances ([Table 1](#)).

However, there still exist some scientific problems and technological challenges that need to be emphasized and resolved. (1) The microscopic kinetic processes in ASSBs are still ambiguous. For instance, it is unclear whether a desolvation-like but undetected process exists at the SE/interphase interface, during which a relatively high energy barrier (similar to desolvation energy) needs to be overcome. (2) The overall low-temperature electrochemical performances, such as capacity retention (relative to room temperature), rate capability and cycle life, are still unsatisfactory, as summarized in [Table 1](#), despite the breakthrough of the lowest working temperature (-60°C). Currently, in terms of the areal loading/capacity and the lowest working temperature, the electrochemical performance of ASSBs using polymer SEs still lags behind that of inorganic SEs. (3) There still remain some divergencies on the identification of resistances from cathode/SE and anode/SE interfaces and those from the interphase layer and charge transfer process, which may impede the reveal of interfacial behaviors.

Based on the in-depth understanding of kinetic processes, low-temperature limitations, and design strategies of ASSBs, several potential directions are proposed here:

- (1) Establishing a low-temperature performance evaluation standard on the critical indicators (e.g., areal capacity $\geq 4 \text{ mAh cm}^{-2}$, current density $\geq 0.8 \text{ mA cm}^{-2}$, capacity retention $\geq 80\%$ at -20°C and $\geq 50\%$ at -40°C to -60°C) to determine the effective working temperature based on the unified charge-discharge protocols;
- (2) Developing accurate and rational impedance analysis method to decouple the interfacial responses from the cathode/SE and anode/SE interface and those from the interphase layer and charge transfer process, and quantify the activation energy of each kinetic process;
- (3) Developing SEs with high ionic conductivity but low activation energy is a prerequisite condition for boosting low-temperature performance;
- (4) Revealing the actual microscopic kinetic process at the interface, as well as the interphase evolution at low temperature;
- (5) Exploring the mechanochemical failure behaviors at low temperature, and accordingly developing strategies to solve/alleviate the interfacial contact issues;
- (6) Exploring the relationships of lithium storage mechanisms and kinetics with low-temperature performances of electrodes, and accordingly designing electrodes with high diffusion coefficient;

Table 1. Summary of the electrochemical performances of ASSBs operating at low temperature

| No. | Battery | Lowest working temperature (°C) | Areal loading (mg/cm ²) | Areal capacity (mAh/cm ²) | Capacity retention vs. RT (%) | Current rate (C) | Current density (mA/cm ²) | Cycles | Ref. |
|-----|--|---------------------------------|-------------------------------------|---------------------------------------|-------------------------------|------------------|---------------------------------------|-------------|-----------------------------|
| 1 | Li-In Li ₆ PS ₅ Cl LNO@NCM523 | -60 (discharge) | 12.5 | 0.6 | ~30 | 0.01 | 0.02 | N/A | Morino ⁵⁰ |
| 2 | In Li ₆ PS ₅ Cl NCM622 | -30 | 14.69 | 1.62 | 60 | 0.02 | 0.053 | N/A | Choi et al. ⁷⁸ |
| 3 | Li-In 65Li ₂ S-30P ₂ S ₅ -5Li ₂ O Li ₃ InCl ₆ NCM622 | -20 | 8.91 | 0.71 | 45.7 | 0.05 | 0.08 | 10 | Ren et al. ⁷⁹ |
| 4 | Li-In Li _{5.6} PS _{4.6} Br _{1.4} NCM622 | -20 | 1.78 | 0.17 | 67.7 | 0.02 | 0.0064 | 20 | Liao et al. ⁸⁰ |
| 5 | Li-In Li _{5.5} PS _{4.5} Cl _{1.5} NCM622 | -20 | 12.7 | 0.53 | 26.6 | 0.5 | 0.8 | 100 | Peng et al. ⁵¹ |
| 6 | Li-In Li ₆ PS ₅ NCM712 | -20 | 2.67 | 0.1 | 23.4 | 0.05 | 0.024 | 20 | He et al. ⁸¹ |
| 7 | Li-In Li _{5.5} PS _{4.5} Cl _{1.5} LNO@NCM712 | -20 | 4.46 | 0.35 | 50.4 | 0.05 | 0.044 | 50 | Peng et al. ⁵⁴ |
| 8 | Li-In Li _{5.5} PS _{4.5} Cl _{1.5} LNO@NCM712 | -20 | 1.82 | 0.16 | 50.0 | 0.05 | 0.016 | 35 | Peng et al. ⁶⁶ |
| 9 | Li-In Li _{5.5} PS _{4.5} Cl _{1.5} NCM811 | -20 | 1.75 | 0.18 | 60.8 | 0.02 | 0.0063 | 25 | Peng et al. ⁸² |
| 10 | Li-In Li _{5.5} PS _{4.425} O _{0.075} Cl _{1.5} NCM811 | -20 | 4.45 | 0.42 | 59.2 | 0.02 | 0.016 | 10 | Peng et al. ⁸³ |
| 11 | μSi Li ₆ PS ₅ Cl NCM811 | -20 (discharge) | N/A | 1.1 | ~36.7 | 0.075 | 0.3 | N/A | Tan et al. ⁷⁶ |
| 12 | LiSH46 Li ₆ PS ₅ Cl NCM811 | 5 | 29.8 | 2.3 | 52.3 | 0.1 | 0.597 | N/A | Yan et al. ⁷⁷ |
| 13 | Li-In Li ₆ PS ₅ Cl Li-LaCeZrHfTa-Cl LiNi _{0.88} Co _{0.09} Mn _{0.03} O ₂ | -30 | 4.45 | 0.45 | 102 | 0.1 | 0.125 | 390 | Li et al. ⁸⁴ |
| 14 | Ag-C Li ₆ PS ₅ Cl Li ₂ O-ZrO ₂ @NCM90(LiNi _{0.90} Co _{0.05} Mn _{0.05} O ₂) | -10 (discharge) | 31.6 | ~3.2 | ~47 | 0.1 | 0.68 | N/A | Lee et al. ¹⁹ |
| 15 | Li-In Li ₆ PS ₅ Cl Li ₃ InCl ₆ NCM(LiNi _{0.90} Co _{0.04} Mn _{0.04} O ₂) | -20 | 4.55 | 0.54 | 54.7 | 0.1 | 0.1 | 100 | Zhang et al. ⁵³ |
| 16 | Li ₄ Ti ₅ O ₁₂ LGPS LNO@LCO | -30 (discharge) | 4.76 | 0.59 (0.44) | ~92.6 (~68.1) | 0.09 (0.9) | 0.06 (0.6) | N/A | Kato et al. ¹⁰ |
| 17 | Li-In Li _{0.54} [Si _{0.6} Ge _{0.4}] _{1.74} P _{1.44} S _{11.1} Br _{0.3} O ₆ LNO@LCO | -10 (discharge) | 167.7 | 17 | 75 | 0.025 | 0.587 | N/A | Li et al. ¹¹ |
| 18 | Li-In Li ₁₀ SnP _{1.84} Sb _{0.16} S _{11.6} O _{0.4} LNO@LCO | -20 | 4.96 | 0.44 | ~75 | 0.1 | 0.069 | N/A | Gao et al. ⁸⁵ |
| 19 | Li-In Li ₆ PS ₅ Cl Li ₃ InCl ₆ LCO | -30 (-10) | 8.91 | 0.89 | 53.8 (74.9) | 0.05 (0.4) | 0.06 (0.48) | 300 | Deng et al. ⁵² |
| 20 | Li-In Li ₆ PS ₅ Cl Li ₃ InCl ₆ LCO GLC@Al | -10 | 4.45 | 0.445 | 75.2 | 0.05 | 0.03 | 100 | Deng et al. ⁵⁹ |
| 21 | Li-In Li ₆ PS ₅ Cl 1.6Li ₂ O-TaCl ₅ LCO | -10 | 8.91 | 0.896 | ~74.5 | 0.1 | 0.125 | 300 | Zhang et al. ⁴² |
| 22 | Li Li ₆ La ₂ Zr _{1.5} Ta _{0.5} O ₁₂ LCO | 10 (discharge) | 8.1 | 0.09 | 20 | 0.05 | 0.0567 | N/A | Yamada et al. ⁶⁸ |
| 23 | Li-In Li ₂ P _{2.8} I _{0.5} Cl _{0.5} 3Li ₂ S-LiI | 0 | 3.18 | 1.83 | 51.5 | N/A | 0.13 | 145 | Wu et al. ⁶⁷ |
| 24 | Li-In Li ₇ P ₃ S ₁₁ FeS ₂ | 0 | 1.53 | 0.56 | 58.7 | 0.05 | 0.057 | 100 | Wang et al. ⁴⁴ |
| 25 | Li-In Li ₆ PS ₅ Cl Mo _{0.5} Ti _{0.5} S ₄ | -40 | 1.99 | 0.92 | 50.7 | 0.1 | 0.14 | 50 (-20°C) | Lu et al. ⁷⁵ |
| 26 | Li-In LASI-80Si FeS ₂ | -60 (-20) | 1.99 | 1.06 | 29.3 (68.9) | 0.1 | 0.15 | N/A | Lu et al. ⁴¹ |
| 27 | Li LCPE-60 LFP | -10 | 1.0 | 0.085 | ~54.1 | 0.1 | 0.017 | 100 | Zhang et al. ⁴⁷ |
| 28 | Li KSCE LFP | 0 | 1.2 | 0.15 | 84.2 | 0.2 | 0.038 | 150 | Lv et al. ⁴⁸ |
| 29 | Li BStSi LFP | -20 (0) | N/A | N/A | 29 (74) | 0.1 | N/A | 300 | Lin and Liu ⁴⁹ |
| 30 | Li TXE-FDMA-LiDFOB NCM811 (quasi-ASSB) | -30 | 3 | 0.282 | ~46.8 | 0.1 | 0.06 | 200 (-20°C) | Li et al. ⁵⁷ |

- (7) Investigating the low-temperature performances of ASSBs based on thick electrodes and large cells (e.g., pouch cells) to promote the practical application;
- (8) Investigating the necessity to employ charge-discharge protocols and thermal management to improve the low-temperature performances of ASSBs further.

Overall, continuous endeavors to overcome the challenges mentioned above are highly desirable to propel the application of ASSBs in cold environments.

ACKNOWLEDGMENTS

We acknowledge the funding support from the Eastern Institute for Advanced Study (EIAS), Eastern Institute of Technology, Ningbo.

DECLARATION OF INTERESTS

The authors declare no competing interests.

REFERENCES

1. Argyrou, M.C., Christodoulides, P., and Kalogirou, S.A. (2018). Energy storage for electricity generation and related processes: Technologies appraisal and grid scale applications. *Renew. Sustain. Energy Rev.* **94**, 804–821.
2. Peng, J., Zu, C., and Li, H. (2013). Fundamental scientific aspects of lithium batteries (I)—Thermodynamic calculations of theoretical energy densities of chemical energy storage systems. *Energy Storage Sci. Technol.* **2**, 55.
3. Wang, Q., Jiang, L., Yu, Y., and Sun, J. (2019). Progress of enhancing the safety of lithium ion battery from the electrolyte aspect. *Nano Energy* **55**, 93–114.
4. Liu, L., Xu, J., Wang, S., Wu, F., Li, H., and Chen, L. (2019). Practical evaluation of energy densities for sulfide solid-state batteries. *eTransportation* **1**, 100010.
5. Chen, R., Li, Q., Yu, X., Chen, L., and Li, H. (2020). Approaching Practically Accessible Solid-State Batteries: Stability Issues Related to Solid Electrolytes and Interfaces. *Chem. Rev.* **120**, 6820–6877.
6. Wu, Y., Wang, S., Li, H., Chen, L., and Wu, F. (2021). Progress in thermal stability of all-solid-state-Li-ion-batteries. *InfoMat* **3**, 827–853.
7. Peng, J., Wu, D., Lu, P., Wang, Z., Du, Y., Wu, Y., Wu, Y., Yan, W., Wang, J., Li, H., et al. (2023). High-safety, wide-temperature-range, low-external-pressure and dendrite-free lithium battery with sulfide solid electrolyte. *Energy Storage Mater.* **54**, 430–439.
8. Janek, J., and Zeier, W.G. (2023). Challenges in speeding up solid-state battery development. *Nat. Energy* **8**, 230–240.
9. Kamaya, N., Homma, K., Yamakawa, Y., Hirayama, M., Kanno, R., Yonemura, M., Kamiyama, T., Kato, Y., Hama, S., Kawamoto, K., et al. (2011). A lithium superionic conductor. *Nat. Mater.* **10**, 682–686.
10. Kato, Y., Hori, S., Saito, T., Suzuki, K., Hirayama, M., Mitsui, A., Yonemura, M., Iba, H., and Kanno, R. (2016). High-power all-solid-state batteries using sulfide superionic conductors. *Nat. Energy* **1**, 1–7.
11. Li, Y., Song, S., Kim, H., Nomoto, K., Kim, H., Sun, X., Hori, S., Suzuki, K., Matsui, N., Hirayama, M., et al. (2023). A lithium superionic conductor for millimeter-thick battery electrode. *Science* **381**, 50–53.
12. Tanaka, Y., Ueno, K., Mizuno, K., Takeuchi, K., Asano, T., and Sakai, A. (2023). New Oxyhalide Solid Electrolytes with High Lithium Ionic Conductivity >10 mS cm⁻¹ for All-Solid-State Batteries. *Angew. Chem. Int. Ed. Engl.* **62**, e202217581.
13. Wu, Z., Li, X., Zheng, C., Fan, Z., Zhang, W., Huang, H., Gan, Y., Xia, Y., He, X., Tao, X., et al. (2023). Interfaces in Sulfide Solid Electrolyte-Based All-Solid-State Lithium Batteries: Characterization, Mechanism and Strategy. *Electrochim. Energy Rev.* **6**, 10.
14. Pang, Y., Pan, J., Yang, J., Zheng, S., and Wang, C. (2021). Electrolyte/Electrode Interfaces in All-Solid-State Lithium Batteries: A Review. *Electrochim. Energy Rev.* **4**, 169–193.
15. Liu, Q., Chen, Q., Tang, Y., and Cheng, H.-M. (2023). Interfacial Modification, Electrode/Solid-Electrolyte Engineering, and Monolithic Construction of Solid-State Batteries. *Electrochim. Energy Rev.* **6**, 15.
16. Lu, P., Liu, L., Wang, S., Xu, J., Peng, J., Yan, W., Wang, Q., Li, H., Chen, L., and Wu, F. (2021). Superior All-Solid-State Batteries Enabled by a Gas-Phase-Synthesized Sulfide Electrolyte with Ultrahigh Moisture Stability and Ionic Conductivity. *Adv. Mater.* **33**, e2100921.
17. Xu, J., Li, Y., Lu, P., Yan, W., Yang, M., Li, H., Chen, L., and Wu, F. (2022). Water-Stable Sulfide Solid Electrolyte Membranes Directly Applicable in All-Solid-State Batteries Enabled by Superhydrophobic Li⁺-Conducting Protection Layer. *Adv. Energy Mater.* **12**, 2102348.
18. Li, Y., Wu, Y., Ma, T., Wang, Z., Gao, Q., Xu, J., Chen, L., Li, H., and Wu, F. (2022). Long-Life Sulfide All-Solid-State Battery Enabled by Substrate-Modulated Dry-Process Binder. *Adv. Energy Mater.* **12**, 2201732.
19. Lee, Y.-G., Fujiki, S., Jung, C., Suzuki, N., Yashiro, N., Omoda, R., Ko, D., Shiratsuchi, T., Sugimoto, T., Ryu, S., et al. (2020). High-energy long-cycling all-solid-state lithium metal batteries enabled by silver–carbon composite anodes. *Nat. Energy* **5**, 299–308.
20. Zhou, L., Zuo, T., Kwok, C.Y., Kim, S.Y., Assoud, A., Zhang, Q., Janek, J., and Nazar, L.F. (2022). High areal capacity, long cycle life 4 V ceramic all-solid-state Li-ion batteries enabled by chloride solid electrolytes. *Nat. Energy* **7**, 83–93.
21. Hou, J., Yang, M., Wang, D., and Zhang, J. (2020). Fundamentals and Challenges of Lithium Ion Batteries at Temperatures between –40 and 60 °C. *Adv. Energy Mater.* **10**, 1904152.
22. Gupta, A., and Manthiram, A. (2020). Designing Advanced Lithium-based Batteries for Low-temperature Conditions. *Adv. Energy Mater.* **10**, 2001972.
23. Zhang, N., Deng, T., Zhang, S., Wang, C., Chen, L., Wang, C., and Fan, X. (2022). Critical Review on Low-Temperature Li-Ion/Metal Batteries. *Adv. Mater.* **34**, e2107899.
24. Piao, N., Gao, X., Yang, H., Guo, Z., Hu, G., Cheng, H., and Li, F. (2022). Challenges and development of lithium-ion batteries for low temperature environments. *eTransportation* **11**, 100145.
25. Jin, C.B., Yao, N., Xiao, Y., Xie, J., Li, Z., Chen, X., Li, B.Q., Zhang, X.Q., Huang, J.Q., and Zhang, Q. (2023). Taming Solvent-Solute Interaction Accelerates Interfacial Kinetics in Low-Temperature Lithium-Metal Batteries. *Adv. Mater.* **35**, e2208340.
26. Hu, A., Li, F., Chen, W., Lei, T., Li, Y., Fan, Y., He, M., Wang, F., Zhou, M., Hu, Y., et al. (2022). Ion Transport Kinetics in Low-Temperature Lithium Metal Batteries. *Adv. Energy Mater.* **12**, 2202432.

27. Hu, Y.-S. (2016). Batteries: Getting solid. *Nat. Energy* 1, 1–2.
28. Huang, J., Wu, K., Xu, G., Wu, M., Dou, S., and Wu, C. (2023). Recent progress and strategic perspectives of inorganic solid electrolytes: fundamentals, modifications, and applications in sodium metal batteries. *Chem. Soc. Rev.* 52, 4933–4995.
29. Ohno, S., Banik, A., Dewald, G.F., Kraft, M.A., Krauskopf, T., Minafra, N., Till, P., Weiss, M., and Zeier, W.G. (2020). Materials design of ionic conductors for solid state batteries. *Prog. Energy* 2, 022001.
30. Wu, S., Xiao, R., Li, H., and Chen, L. (2022). New insights into the mechanism of cation migration induced by cation–anion dynamic coupling in superionic conductors. *J. Mater. Chem. A* 10, 3093–3101.
31. Lau, J., DeBlock, R.H., Butts, D.M., Ashby, D.S., Choi, C.S., and Dunn, B.S. (2018). Sulfide Solid Electrolytes for Lithium Battery Applications. *Adv. Energy Mater.* 8, 1800933.
32. Anderson, O.L., and Stuart, D.A. (1954). Calculation of Activation Energy of Ionic Conductivity in Silica Glasses by Classical Methods. *J. Am. Ceram. Soc.* 37, 573–580.
33. Kim, Y., and Martin, S. (2006). Ionic conductivities of various Ge₂-based oxy-sulfide amorphous materials prepared by melt-quenching and mechanical milling methods. *Solid State Ionics* 177, 2881–2887.
34. An, Y., Han, X., Liu, Y., Azhar, A., Na, J., Nanjundan, A.K., Wang, S., Yu, J., and Yamauchi, Y. (2022). Progress in Solid Polymer Electrolytes for Lithium-Ion Batteries and Beyond. *Small* 18, e2103617.
35. Zhang, D., Meng, X., Hou, W., Hu, W., Mo, J., Yang, T., Zhang, W., Fan, Q., Liu, L., Jiang, B., et al. (2023). Solid polymer electrolytes: Ion conduction mechanisms and enhancement strategies. *Nano Res. Energy* 2, e9120050.
36. Hu, C., Shen, Y., Shen, M., Liu, X., Chen, H., Liu, C., Kang, T., Jin, F., Li, L., Li, J., et al. (2020). Superionic Conductors via Bulk Interfacial Conduction. *J. Am. Chem. Soc.* 142, 18035–18041.
37. Li, Z., Fu, J., Zhou, X., Gui, S., Wei, L., Yang, H., Li, H., and Guo, X. (2023). Ionic Conduction in Polymer-Based Solid Electrolytes. *Adv. Sci. (Weinh)* 10, e2201718.
38. Xu, K., von Cresce, A., and Lee, U. (2010). Differentiating contributions to "ion transfer" barrier from interphasial resistance and Li⁺ desolvation at electrolyte/graphite interface. *Langmuir* 26, 11538–11543.
39. Belgibayeva, A., Rakhatmetova, A., Rakhatkyzy, M., Kairova, M., Mukushev, I., Issatayev, N., Kalimuldina, G., Nurpeissova, A., Sun, Y., and Bakenov, Z. (2023). Lithium-ion batteries for low-temperature applications: Limiting factors and solutions. *J. Power Sources* 557, 232550.
40. Lu, Y., Zhao, C.-Z., Huang, J.-Q., and Zhang, Q. (2022). The timescale identification decoupling complicated kinetic processes in lithium batteries. *Joule* 6, 1172–1198.
41. Lu, P., Xia, Y., Huang, Y., Li, Z., Wu, Y., Wang, X., Sun, G., Shi, S., Sha, Z., Chen, L., et al. (2023). Wide-Temperature, Long-Cycling, and High-Loading Pyrite All-Solid-State Batteries Enabled by Argyrodite Thioarsenate Superionic Conductor. *Adv. Funct. Mater.* 33, 2211211.
42. Zhang, S., Zhao, F., Chen, J., Fu, J., Luo, J., Alahakoon, S.H., Chang, L.Y., Feng, R., Shakouri, M., Liang, J., et al. (2023). A family of oxychloride amorphous solid electrolytes for long-cycling all-solid-state lithium batteries. *Nat. Commun.* 14, 3780.
43. Lu, P., Xia, Y., Sun, G., Wu, D., Wu, S., Yan, W., Zhu, X., Lu, J., Niu, Q., Shi, S., et al. (2023). Realizing long-cycling all-solid-state Li-In||TiS₂ batteries using Li_{6+x}M_xAs_{1-x}Si₁ (M=Si, Sn) sulfide solid electrolytes. *Nat. Commun.* 14, 4077.
44. Wang, R., Wu, Z., Yu, C., Wei, C., Peng, L., Wang, L., Cheng, S., and Xie, J. (2023). Low temperature ensures FeS₂ cathode a superior cycling stability in Li₇P₃S₁₁-based all-solid-state lithium batteries. *Front. Energy Res.* 10, 1108789.
45. Wu, J., Liu, S., Han, F., Yao, X., and Wang, C. (2021). Lithium/Sulfide All-Solid-State Batteries using Sulfide Electrolytes. *Adv. Mater.* 33, e2000751.
46. Wu, F., Zhang, K., Liu, Y., Gao, H., Bai, Y., Wang, X., and Wu, C. (2020). Polymer electrolytes and interfaces toward solid-state batteries: Recent advances and prospects. *Energy Storage Mater.* 33, 26–54.
47. Zhang, X., Fu, C., Cheng, S., Zhang, C., Zhang, L., Jiang, M., Wang, J., Ma, Y., Zuo, P., Du, C., et al. (2023). Novel PEO-based composite electrolyte for low-temperature all-solid-state lithium metal batteries enabled by interfacial cation-assistance. *Energy Storage Mater.* 56, 121–131.
48. Lv, F., Liu, K., Wang, Z., Zhu, J., Zhao, Y., and Yuan, S. (2021). Ultraviolet-cured polyethylene oxide-based composite electrolyte enabling stable cycling of lithium battery at low temperature. *J. Colloid Interface Sci.* 596, 257–266.
49. Lin, Z., and Liu, J. (2019). Low-temperature all-solid-state lithium-ion batteries based on a di-cross-linked starch solid electrolyte. *RSC Adv.* 9, 34601–34606.
50. Morino, Y. (2022). Impact of Surface Coating on the Low Temperature Performance of a Sulfide-Based All-Solid-State Battery Cathode. *Electrochemistry* 90, 27001–27001.
51. Peng, L., Yu, C., Zhang, Z., Ren, H., Zhang, J., He, Z., Yu, M., Zhang, L., Cheng, S., and Xie, J. (2022). Chlorine-rich lithium argyrodite enabling solid-state batteries with capabilities of high voltage, high rate, low-temperature and ultralong cyclability. *Chem. Eng. J.* 430, 132896.
52. Deng, S., Jiang, M., Chen, N., Li, W., Zheng, M., Chen, W., Li, R., Huang, H., Wang, J., Singh, C.V., et al. (2022). Regulating Electronic Conductivity at Cathode Interface for Low-Temperature Halide-Based All-Solid-State Batteries. *Adv. Funct. Mater.* 32, 2205594.
53. Zhang, Z., Jia, W., Feng, Y., Ai, R., Yu, J., Bie, X., Zhai, X., Jiang, T., Yao, S., and Du, F. (2023). An ultraconformal chemo-mechanical stable cathode interface for high-performance all-solid-state batteries at wide temperatures. *Energy Environ. Sci.* 16, 4453–4463.
54. Peng, L., Ren, H., Zhang, J., Chen, S., Yu, C., Miao, X., Zhang, Z., He, Z., Yu, M., Zhang, L., et al. (2021). LiNbO₃-coated LiNi_{0.7}Co_{0.1}Mn_{0.2}O₂ and chlorine-rich argyrodite enabling high-performance solid-state batteries under different temperatures. *Energy Storage Mater.* 43, 53–61.
55. Bong, W.S.K., Shiota, A., Miwa, T., Morino, Y., Kanada, S., and Kawamoto, K. (2023). Effect of thickness and uniformity of LiNbO₃-coated layer on LiNi_{0.5}Co_{0.2}Mn_{0.3}O₂ cathode material on enhancement of cycle performance of full-cell sulfide-based all-solid-state batteries. *J. Power Sources* 577, 233259.
56. Morino, Y., Shiota, A., Kanada, S., Bong, W.S.K., Kawamoto, K., Inda, Y., Tsukasaki, H., Mori, S., and Iriyama, Y. (2023). Design of Cathode Coating Using Niobate and Phosphate Hybrid Material for Sulfide-Based Solid-State Battery. *ACS Appl. Mater. Interfaces* 15, 36086–36095.
57. Li, Z., Yu, R., Weng, S., Zhang, Q., Wang, X., and Guo, X. (2023). Tailoring polymer electrolyte ionic conductivity for production of low-temperature operating quasi-all-solid-state lithium metal batteries. *Nat. Commun.* 14, 482.
58. Yu, C., Zhao, F., Luo, J., Zhang, L., and Sun, X. (2021). Recent development of lithium argyrodite solid-state electrolytes for solid-state batteries: Synthesis, structure, stability and dynamics. *Nano Energy* 83, 105858.
59. Deng, S., Jiang, M., Rao, A., Lin, X., Doyle-Davis, K., Liang, J., Yu, C., Li, R., Zhao, S., Zhang, L., et al. (2022). Fast-Charging Halide-Based All-Solid-State Batteries by Manipulation of Current Collector Interface. *Adv. Funct. Mater.* 32, 2200767.
60. Tan, D.H.S., Wu, E.A., Nguyen, H., Chen, Z., Marple, M.A.T., Doux, J., Wang, X., Yang, H., Banerjee, A., and Meng, Y.S. (2019). Elucidating Reversible Electrochemical Redox of Li₆PS₅Cl Solid Electrolyte. *ACS Energy Lett.* 4, 2418–2427.
61. Han, F., Gao, T., Zhu, Y., Gaskell, K.J., and Wang, C. (2015). A Battery Made from a Single Material. *Adv. Mater.* 27, 3473–3483.
62. Walther, F., Randau, S., Schneider, Y., Sann, J., Rohnke, M., Richter, F.H., Zeier, W.G., and Janek, J. (2020). Influence of Carbon Additives on the Decomposition Pathways in Cathodes of Lithium Thiophosphate-Based All-Solid-State Batteries. *Chem. Mater.* 32, 6123–6136.
63. Hakari, T., Deguchi, M., Mitsuhashi, K., Ohta, T., Saito, K., Orikasa, Y., Uchimoto, Y., Kowada, Y., Hayashi, A., and Tatsumisago, M. (2017). Structural and Electronic-State Changes of a Sulfide Solid Electrolyte during the Li Deinsertion–Insertion Processes. *Chem. Mater.* 29, 4768–4774.
64. Deng, S., Sun, Y., Li, X., Ren, Z., Liang, J., Doyle-Davis, K., Liang, J., Li, W., Norouzi Banis, M., Sun, Q., et al. (2020). Eliminating the Detrimental Effects of Conductive Agents in Sulfide-Based Solid-State Batteries. *ACS Energy Lett.* 5, 1243–1251.
65. Huang, S., Cheong, L.-Z., Wang, D., and Shen, C. (2018). Thermal stability of solid electrolyte

- interphase of lithium-ion batteries. *Appl. Surf. Sci.* 454, 61–67.
66. Peng, L., Yu, C., Zhang, Z., Xu, R., Sun, M., Zhang, L., Cheng, S., and Xie, J. (2023). Tuning Solid Interfaces via Varying Electrolyte Distributions Enables High-Performance Solid-State Batteries. *Energy Environ. Mater.* 6, 12308.
67. Wu, Z., Chen, S., Yu, C., Wei, C., Peng, L., Wang, H., Cheng, S., and Xie, J. (2022). Engineering high conductive Li₇P₂S₈ via Cl⁻ doping for all-solid-state Li-S batteries workable at different operating temperatures. *Chem. Eng. J.* 442, 136346.
68. Yamada, H., Ito, T., Nakamura, T., Bekarevich, R., Mitsuishi, K., Kammampata, S.P., and Thangadurai, V. (2023). High Cathode Loading and Low-Temperature Operating Garnet-Based All-Solid-State Lithium Batteries – Material/Process/Architecture Optimization and Understanding of Cell Failure. *Small* 19, e2301904.
69. Zhao, Q., Liu, X., Stalin, S., Khan, K., and Archer, L.A. (2019). Solid-state polymer electrolytes with in-built fast interfacial transport for secondary lithium batteries. *Nat. Energy* 4, 365–373.
70. LePage, W.S., Chen, Y., Kazyak, E., Chen, K., Sanchez, A.J., Poli, A., Arruda, E.M., Thouless, M.D., and Dasgupta, N.P. (2019). Lithium Mechanics: Roles of Strain Rate and Temperature and Implications for Lithium Metal Batteries. *J. Electrochem. Soc.* 166, A89–A97.
71. Spencer Jolly, D., Ning, Z., Hartley, G.O., Liu, B., Melvin, D.L.R., Adamson, P., Marrow, J., and Bruce, P.G. (2021). Temperature Dependence of Lithium Anode Voiding in Argyrodite Solid-State Batteries. *ACS Appl. Mater. Interfaces* 13, 22708–22716.
72. Papakyriakou, M., Lu, M., Liu, Y., Liu, Z., Chen, H., McDowell, M.T., and Xia, S. (2021). Mechanical behavior of inorganic lithium-conducting solid electrolytes. *J. Power Sources* 516, 230672.
73. Lin, Zejing, Mao, M., Yang, C., Tong, Y., Li, Q., Yue, J., Yang, G., Zhang, Q., Hong, L., Yu, X., et al. (2021). Amorphous anion-rich titanium polysulfides for aluminum-ion batteries. *Sci. Adv.* 7, eabg6314.
74. Sakuda, A., Ohara, K., Fukuda, K., Nakanishi, K., Kawaguchi, T., Arai, H., Uchimoto, Y., Ohta, T., Matsubara, E., Ogumi, Z., et al. (2017). Amorphous Metal Polysulfides: Electrode Materials with Unique Insertion/Extraction Reactions. *J. Am. Chem. Soc.* 139, 8796–8799.
75. Lu, P., Gong, S., Guo, F., Zhu, X., Huang, Y., Wang, Y., He, W., Yang, M., Chen, L., Li, H., et al. (2023). Amorphous bimetallic polysulfide for all-solid-state batteries with superior capacity and low-temperature tolerance. *Nano Energy* 118, 109029.
76. Tan, D.H.S., Chen, Y.T., Yang, H., Bao, W., Sreenarayanan, B., Doux, J.M., Li, W., Lu, B., Ham, S.Y., Sayahpour, B., et al. (2021). Carbon-free high-loading silicon anodes enabled by sulfide solid electrolytes. *Science* 373, 1494–1499.
77. Yan, W., Mu, Z., Wang, Z., Huang, Y., Wu, D., Lu, P., Lu, J., Xu, J., Wu, Y., Ma, T., et al. (2023). Hard-carbon-stabilized Li-Si anodes for high-performance all-solid-state Li-ion batteries. *Nat. Energy* 8, 800–813.
78. Choi, S., Jeon, M., Kim, B.K., Sang, B.I., and Kim, H. (2018). Electrochemical behaviors of Li-argyrodite-based all-solid-state batteries under deep-freezing conditions. *Chem. Commun. (Camb)* 54, 14116–14119.
79. Ren, H.-T., Zhang, Z., Zhang, J., Peng, L., He, Z., Yu, M., Yu, C., Zhang, L., Xie, J., and Cheng, S. (2022). Improvement of stability and solid-state battery performances of annealed 70Li₂S–30P₂S₅ electrolytes by additives. *Rare Met.* 41, 106–114.
80. Liao, C., Yu, C., Miao, X., Chen, S., Peng, L., Wei, C., Wu, Z., Cheng, S., and Xie, J. (2022). Synthesis of Br-rich argyrodite electrolytes enables all-solid-state batteries with superior battery performances at different operating temperatures. *Materialia* 26, 101603.
81. He, Z.-Y., Zhang, Z., Yu, M., Yu, C., Ren, H., Zhang, J., Peng, L., Zhang, L., Cheng, S., and Xie, J. (2022). Synthetic optimization and application of Li-argyrodite Li₆PS₅I in solid-state battery at different temperatures. *Rare Met.* 41, 798–805.
82. Peng, L., Chen, S., Yu, C., Liao, C., Sun, M., Wang, H., Zhang, L., Cheng, S., and Xie, J. (2022). Unraveling the crystallinity on battery performances of chlorine-rich argyrodite electrolytes. *J. Power Sources* 520, 230890.
83. Peng, L., Chen, S., Yu, C., Wei, C., Liao, C., Wu, Z., Wang, H.L., Cheng, S., and Xie, J. (2022). Enhancing Moisture and Electrochemical Stability of the Li₅PS_{4.5}Cl_{1.5} Electrolyte by Oxygen Doping. *ACS Appl. Mater. Interfaces* 14, 4179–4185.
84. Li, X., Xu, Y., Zhao, C., Wu, D., Wang, L., Zheng, M., Han, X., Zhang, S., Yue, J., Xiao, B., et al. (2023). The Universal Super Cation-Conductivity in Multiple-cation Mixed Chloride Solid-State Electrolytes. *Angew. Chem. Int. Ed. Engl.* 62, e202306433.
85. Gao, J., Sun, X., Wang, C., Zhang, Y., Yang, L., Song, D., Wu, Y., Yang, Z., Ohsaka, T., Matsumoto, F., et al. (2022). Sb- and O-Cosubstituted Li₁₀SnP₂S₁₂ with High Electrochemical and Air Stability for All-Solid-State Lithium Batteries. *ChemElectroChem* 9, e202200156.